

Improved Consensus ADMM for Cooperative Motion Planning of Large-Scale Connected Autonomous Vehicles with Limited Communication

Haichao Liu, Zhenmin Huang, Zicheng Zhu, Yulin Li, Shaojie Shen, and Jun Ma

Abstract—This paper investigates a cooperative motion planning problem for large-scale connected autonomous vehicles (CAVs) under limited communications, which addresses the challenges of high communication and computing resource requirements. Our proposed methodology incorporates a parallel optimization algorithm with improved consensus ADMM considering a more realistic locally connected topology network, and time complexity of $O(N)$ is achieved by exploiting the sparsity in the dual update process. To further enhance the computational efficiency, we employ a lightweight evolution strategy for the dynamic connectivity graph of CAVs, and each sub-problem split from the consensus ADMM only requires managing a small group of CAVs. The proposed method implemented with the receding horizon scheme is validated thoroughly, and comparisons with existing numerical solvers and approaches demonstrate the efficiency of our proposed algorithm. Also, simulations on large-scale cooperative driving tasks involving 80 vehicles are performed in the high-fidelity CARLA simulator, which highlights the remarkable computational efficiency, scalability, and effectiveness of our proposed development. Demonstration videos are available at https://henryhliu.github.io/icadmm_cmp_carla.

Index Terms—Connected autonomous vehicles (CAVs), cooperative motion planning, alternating direction method of multipliers (ADMM), iterative linear quadratic regulator (iLQR).

I. INTRODUCTION

Recent developments in wireless communications and intelligent transportation systems, particularly the integration of autonomous driving with vehicle-to-everything (V2X) technologies, have provided valuable insights in addressing urban transportation challenges [1], [2]. Additionally, advanced planning and control methodologies for multi-agent systems have shown significant potential in the field of autonomous vehicles [3], [4]. As a result, connected autonomous vehicles (CAVs) have emerged as a promising technological solution for reducing traffic congestion, preventing accidents, and enhancing both driving safety and efficiency. Significantly,

Haichao Liu, Zhenmin Huang, Yulin Li, and Jun Ma are with the Robotics and Autonomous Systems Thrust and the Department of Electronic and Computer Engineering, The Hong Kong University of Science and Technology, China (e-mail: hliu369@connect.ust.hk; zhuangdf@connect.ust.hk; yline@connect.ust.hk; jun.ma@ust.hk).

Zicheng Zhu is with the Department of Electrical and Computer Engineering, National University of Singapore, Singapore (e-mail: zhuzicheng@u.nus.edu)

Shaojie Shen is with the Department of Electronic and Computer Engineering, The Hong Kong University of Science and Technology, China (e-mail: eeshaojie@ust.hk).

This work has been submitted to the IEEE for possible publication. Copyright may be transferred without notice, after which this version may no longer be accessible.



Fig. 1. Demonstration of the proposed collaborative motion planning strategy for large-scale CAVs in urban driving scenarios. The problem is formulated, where one optimal control problem is constructed within each subgraph (orange region) and solved by the improved consensus ADMM algorithm. The subgraphs are generated by the proposed graph evolution algorithm, in which the edges of the dynamic connectivity graph are created within each blue region centered by each CAV within a specified subgraph.

achieving cooperative driving is a multi-faced endeavor that involves various essential aspects, including environmental perception [5], global path generation [6], motion planning [7], trajectory tracking control [8], etc. Within the framework of cooperative motion planning, CAVs collaboratively make joint decisions and subsequently generate cooperative trajectories aimed at optimizing overall system performance and ensuring safe and efficient maneuvers. However, the incorporation of various key factors, such as inter-vehicle collision avoidance, vehicle model, and various physical constraints, renders cooperative motion planning a challenging task. This is especially evident when dealing with a larger number of CAVs or when operating in complex traffic environment. To address the cooperative motion planning problem for CAVs, a series of representative works have been presented, drawing inspiration from advancements in both learning-based and optimization-based methodologies [9].

The use of learning-based algorithms, represented by reinforcement learning (RL), has become prevalent in tackling motion planning problems [10], [11]. In the context of multi-agent path finding, PRIMAL serves as a decentralized framework that plans efficient single-agent paths by imitating a centralized expert through imitation learning, thereby facilitating implicit coordination during online path planning [12]. Despite its

scalability to larger teams, PRIMAL suffers from performance deterioration in structured and densely occupied environments that require substantial efforts in coordination of agents. To address this limitation, drawing inspiration from slime mold, RL-APCP³ presents an effective solution to the deterioration problem in dense maps using bionic SARSA algorithm [13]. Specifically for CAVs, a learning-based iterative optimization algorithm was used to explore the collision-free cooperative motion planning problem for CAVs at unsignalized intersections [14]. In addition, a novel multi-agent behavioral planning scheme for CAVs was investigated by exploiting RL and graph neural networks at urban intersections, which improves the vehicle throughput significantly [15]. However, the learning-based methods typically require substantial real-world data and may be limited by their interpretability, restricting their generalization to a wider range of traffic scenarios.

Alternatively, optimization-based approaches commonly adopt an optimal control problem (OCP) formulation for motion planning tasks. This approach offers several benefits such as providing a precise mathematical representation, ensuring interpretability, and proving optimality [16]. When dealing with cooperative motion planning problems involving CAVs with nonlinear vehicle models, these OCPs can be typically solved using well-established nonlinear programming solvers such as interior point optimizer (IPOPT) and sequential quadratic programming (SQP). Additionally, the iterative linear quadratic regulator (iLQR) leverages the benefits of differential dynamic programming (DDP) for addressing nonlinear optimization problems, while retaining only the first-order term of dynamics through Gauss-Newton approximation to enhance the computational efficiency [17]. While the traditional iLQR algorithm is effective and efficient in handling system dynamic constraints, this method cannot directly address various inequality constraints entailed by collision avoidance requirements and other physical limitations. To overcome this limitation, many representative works have been presented to cope with inequality constraints within the DDP/iLQR framework, including control-limited DDP [18], [19] and constrained iLQR [20]–[22]. To further reduce the computational burden, especially for large-scale systems, the alternating direction method of multipliers (ADMM) was developed by decomposing the original optimization problem into several sub-problems [23]. With its parallel and distributed characteristics, the ADMM can be well-suited to address the cooperative motion planning problem for CAVs [24]. Leveraging the dual consensus ADMM [25], a fully parallel optimization framework was established for cooperative trajectory planning of CAVs, which effectively distributes the computational load evenly among all participants, allowing for real-time performance [26].

However, the aforementioned works rely on a strong assumption of fully connected topology network between CAVs, which is not applicable in real-world driving conditions under V2X communication, due to high delays and low transmission reliability associated with long-range and large-scale V2X communication [27]. To address the communication delays, the QuAsyADMM algorithm that incorporates a finite time quantized averaging approach was proposed, and it achieves

the performance comparable to that of algorithms under the perfect communication [28]. On the other hand, decentralized methods have also been explored, utilizing ADMM applied to the dual of the resource allocation problem, where each agent exchanges information solely with its neighbors [25], [29]. The convergence of this method has been proven, and its effectiveness has been illustrated through numerical examples. Building upon the aforementioned algorithm, the ND-DDP algorithm was presented, where an efficient three-level architecture was proposed employing ADMM for consensus and DDP for scalability [30]. With this approach, only local communication is required. However, these solutions, which focus on commuting with neighbors, exhibit long computational time when the number of agents increases. Also, these approaches only consider a graph that does not evolve with time, where the assigned neighbors of each agent are assumed to be fixed. Yet in the real-world urban driving scenarios, the topology network between vehicles is spatiotemporally dynamic, with each node experiencing constantly fast changing neighborhoods throughout the driving process [31]. Nonetheless, maintaining a dynamic connectivity graph within the whole planning horizon is challenging considering the uncertainty in the future trajectories of all vehicles. Fortunately, receding horizon frameworks formulated with the model predictive control (MPC), offer the potential for more robust driving performance [32], [33]. Nonetheless, solving a centralized MPC problem involving all the agents is rather time-consuming [34]. Alternatively, the distributed MPC has also been widely deployed [35], [36], in which each agent only considers its own objective thereby obviously reducing the scale of optimization. In [37], a partially parallel computation framework is proposed to solve the multi-agent MPC problem based on ADMM. However, even if all agents can be deployed in a distributed manner, the collision avoidance requirements (which naturally lead to the coupling effects among agents) result in a dramatic increase in the number of constraints to the optimization problem. Therefore, all these aforementioned methods suffer from significant computational burdens, rendering them difficult to deploy in large-scale CAVs. Apparently, to establish an efficient cooperative driving framework for an excessive number of CAVs, necessary efforts are required to decompose the overall OCP into a series of fully parallel and solvable sub-problems, such that the problem can be solved efficiently.

Driven by the aforementioned challenges, this paper introduces an improved consensus ADMM for cooperative motion planning of large-scale CAVs with locally connected topology network, together with a graph evolution strategy to limit the scale of each OCP corresponding to each subset of the CAVs. The overview of the proposed methodology is demonstrated in Fig. 1. Particularly, to achieve high computational efficiency, we transform and decouple the inter-vehicle constraints and leverage parallel solving capabilities of the ADMM. Moreover, we reduce the complexity of the dual update process by capturing the sparsity of the problem and deriving a simplified equivalent form. Furthermore, we improve its real-time performance by limiting the scale of the optimization problem by integrating the dynamic graph evolution algorithm.

The key contributions of this work are as follows:

- An improved consensus ADMM algorithm is introduced to solve the cooperative motion planning problem with a locally connected topology network, such that the problem is decomposed into a series of sub-problems that can be solved in a parallel manner. This algorithm achieves a complexity of $\mathcal{O}(N)$ by exploiting the sparsity in the dual update process.
- A graph evolution strategy for a dynamic connectivity graph of CAVs is presented to characterize the interaction patterns among CAVs, and each sub-problem attempts to manage a small group of CAVs. In this sense, the computational efficiency can be further enhanced.
- A closed-loop framework for cooperative motion planning is then proposed, which integrates the graph evolution in a receding horizon fashion. This enhances the ability of consensus ADMM to cope with large-scale CAVs and provides a more robust driving performance.
- Real-time performance and superiority of our proposed method is demonstrated through numerical simulations. The large-scale cooperative motion planning simulations involving 80 CAVs are executed in a high-fidelity urban map in CARLA, and the results showcase the effectiveness and robustness of our proposed methodology.

The rest of this paper is organized as follows: Section II provides the definitions of notations. In Section III, we present the CAVs' connectivity pattern using graph theory and formulate the cooperative motion planning problem. Section IV reformulates the problem and an improved consensus ADMM is proposed. In Section V, we present a closed-loop receding horizon-based cooperative motion planning strategy based on our graph evolution algorithm. In Section VI, we demonstrate the performance of the proposed methodology through a series of simulations. Section VII presents the conclusion.

II. NOTATIONS

We use the lowercase letter and uppercase letter to represent a vector $\mathbf{x} \in \mathbb{R}^n$ and a matrix $\mathbf{X} \in \mathbb{R}^{n \times m}$, respectively. Also, $\text{diag}\{a_1, a_2, \dots, a_n\}$ represents a diagonal matrix with $a_i, i \in \{1, 2, \dots, n\}$ as diagonal entries. Similarly, $\text{blddiag}\{\mathbf{A}_1, \mathbf{A}_2, \dots, \mathbf{A}_n\}$ is used to represent a block diagonal matrix with block diagonal entries $\mathbf{A}_1, \mathbf{A}_2, \dots, \mathbf{A}_n$. The sets of non-negative integers and real numbers are represented as \mathbb{Z}_+ and \mathbb{R}_+ , respectively. A logical/Boolean matrix is denoted as \mathbb{B} . $[\cdot]^i$ represents the variable of the i th CAV, while $[\cdot]_\tau$ indicates the variable at time step τ . For simplicity, a matrix concatenated in row $[\mathbf{s}^1, \mathbf{s}^2, \dots, \mathbf{s}^n]$ is denoted as $[\mathbf{s}^i], i = 1, 2, \dots, n$. On the contrary, we denote the matrix with entries \mathbf{s}^i concatenated by column as $[\mathbf{s}^1; \mathbf{s}^2; \dots; \mathbf{s}^n]$. The squared weighted L_2 -norm $\mathbf{x}^T \mathbf{M} \mathbf{x}$ is simplified as $\|\mathbf{x}\|_{\mathbf{M}}^2$. We denote an *indicator function* w.r.t. a set $\mathcal{X} \in \mathbb{R}^n$ as $\mathcal{I}_{\mathcal{X}}(\mathbf{x})$, which takes value 0 if $\mathbf{x} \in \mathbb{R}^n$ belongs to \mathcal{X} and $+\infty$ otherwise. Element-wise maximization and minimization operations for the vectors \mathbf{a} and \mathbf{b} are denoted as $\max\{\mathbf{a}, \mathbf{b}\}$ and $\min\{\mathbf{a}, \mathbf{b}\}$, respectively.

III. PROBLEM FORMULATION

A. Representation of CAVs with Graph Theory

The relationship of CAVs can be represented using graph theory, where nodes represent individual vehicles and edges represent communication links between them. This representation allows for a comprehensive analysis of the communication relationships among CAVs. Let $\mathcal{G} = (\mathcal{V}, \mathcal{E})$ be an undirected graph, where \mathcal{V} represents the set of vehicles and \mathcal{E} represents the set of communication links between nodes. Each vehicle $n^i \in \mathcal{V}$ is associated with a state vector \mathbf{z}^i and a control input vector \mathbf{u}^i . It is pertinent to note that according to the relative locations of the CAVs, the subgraphs of \mathcal{G} are noted as \mathcal{H} , evolved between the planning horizons of cooperative driving. Particularly, even in the same subgraph, the vehicle n^i only exchanges information with its surrounding vehicles within a certain communication range. For clarification, we denote the number of CAVs in the whole traffic system as M . Accordingly, the distance matrix $\mathbf{D} = [a_{ij}] \in \mathbb{R}^{M \times M}$ with $i, j \in \{1, 2, \dots, M\}$ of the whole connectivity graph \mathcal{G} can be formulated. The number of CAVs in each subgraph $\mathcal{H}_k = (\mathcal{N}_k, \mathcal{E}_{k,h})$ is denoted as N_k . Note that we omit the subscript k (the index of a subgraph) of the above notations by default for simplicity. As shown in Fig. 1, for each pair of vehicles, an edge $(n^i, n^j) = d^{i,j} \in \mathcal{E}_h \subseteq \mathcal{E}$ is established if the distance between the pair of vehicles $d^{i,j}$ is smaller than the communication range $r_{\text{tele}}^i \in \mathbb{R}_+$. In addition, we define the cardinality of a node n^i in \mathcal{H} as $|n^i| = \text{deg}(n^i)$, describing the number of indices of the connected non-self nodes in

$$\mathcal{N}^i = \{j \in \mathcal{N} \mid (i, j) \in \mathcal{E}_h\}. \quad (1)$$

The above representation offers clear and logical insights into the connectivity and communication patterns among CAVs, thereby aiding the practical implementation of decentralized cooperative motion planning algorithms.

B. Vehicle Model

For all CAVs, the non-linear bicycle kinematics model in [38] is used. The state vector of a vehicle is $\mathbf{z} = [x, y, \theta, v]^T$, where x and y are the positions of the rear axle of the vehicle from x -axis and y -axis in the global Cartesian map, θ and v are the heading angle (from the positive direction of the x -axis) and velocity of the vehicle, respectively. The control input vector is $\mathbf{u} = [a, \delta]^T$, where a and δ are the acceleration and steering angle of the front wheel, respectively. Then, the vehicle model can be expressed as:

$$\mathbf{z}_{\tau+1} = f(\mathbf{z}_\tau, \mathbf{u}_\tau) = \begin{bmatrix} x_\tau + f_i(v_\tau, \delta_\tau) \cos \theta_\tau \\ y_\tau + f_i(v_\tau, \delta_\tau) \sin \theta_\tau \\ \theta_\tau + \arcsin\left(\frac{g(v_\tau, \delta_\tau)}{b_i}\right) \\ v_\tau + \tau_s a_\tau \end{bmatrix}, \quad (2)$$

where $g(v, \delta) = v_\tau \Delta T \sin(\delta_\tau)$, $f_i(v, \delta)$ is defined as:

$$f_i(v, \delta) = b_i + v \Delta T \cos \delta - \sqrt{b_i^2 - g(v, \delta)^2}, \quad (3)$$

where b_i is the wheelbase of the i th CAV and $\Delta T = 0.1$ s. In addition, we formulate two matrices to denote the state vectors and control inputs of the i th CAV by

$$\mathbf{Z}^i = \{\mathbf{z}_0^i, \mathbf{z}_1^i, \dots, \mathbf{z}_T^i\}, \mathbf{U}^i = \{\mathbf{u}_0^i, \mathbf{u}_1^i, \dots, \mathbf{u}_{T-1}^i\}.$$

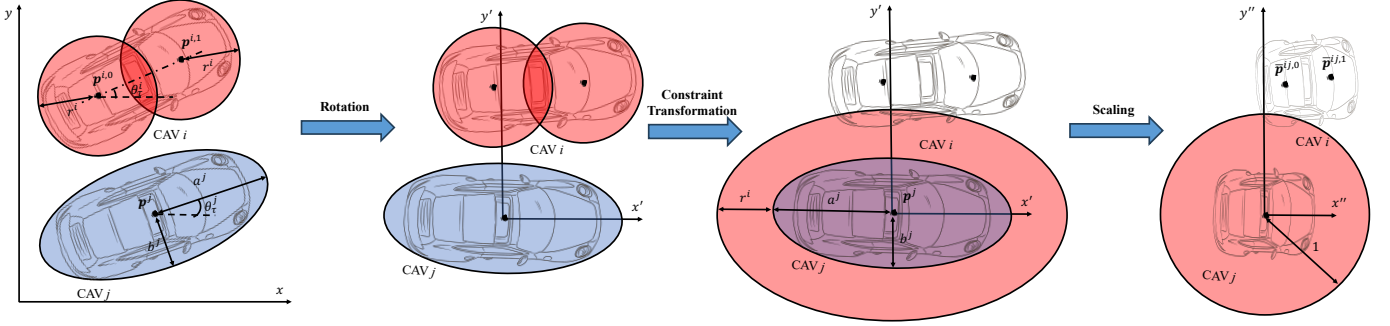


Fig. 2. Geometric relationship and transformation for inter-vehicle collision avoidance, in which the two CAVs in a pair are enveloped with a double circle and an ellipse, respectively. The radius of CAV i is r^i , while the length of semi-major and semi-minor axes of CAV j are a^j and b^j , respectively. The rotation angle between the global coordinate system and the a -parallel coordinate system is the same as the heading angle of the θ^j . After the above transformation, the collision discriminant becomes judging whether a point is within a unit circle.

C. Cooperative Motion Planning with Communication Limits

This work considers a cooperative motion planning task in one subgraph \mathcal{H} where N CAVs drive on the urban road with their destinations and global path. Assuming all the vehicles share the same control and velocity limits, we formulate this problem as an OCP:

$$\begin{aligned}
 \min_{\mathbf{z}_\tau^i, \mathbf{u}_\tau^i} \quad & \sum_{i=1}^N Q_i(\mathbf{Z}^i, \mathbf{U}^i) \\
 \text{s.t.} \quad & \mathbf{z}_{\tau+1}^i = f(\mathbf{z}_\tau^i, \mathbf{u}_\tau^i), \\
 & \mathbf{z}_{\tau+1}^i \in \mathcal{S}_\tau^i, \\
 & -\mathbf{u}^i \leq \mathbf{u}_\tau^i \leq \bar{\mathbf{u}}^i, \\
 & -\underline{\mathbf{z}}^i \leq \mathbf{z}_\tau^i \leq \bar{\mathbf{z}}^i, \\
 & -\underline{\mathbf{z}}^i \leq \mathbf{z}_T^i \leq \bar{\mathbf{z}}^i, \\
 & \forall \tau \in \mathcal{T}, \forall i \in \mathcal{N},
 \end{aligned} \quad (4)$$

where \mathcal{N} represents the set of index of CAVs in the traffic system of a subgraph \mathcal{H} . $\mathcal{T} = \{0, 1, \dots, T-1\}$ is the temporal horizon within a cooperative motion planning episode. In addition, \mathcal{S}_τ^i is the collision-free region of the i th CAV at time step τ , which will be defined in Section III-D. \mathbf{u}^i and $\bar{\mathbf{u}}^i$ mean the lower and upper bound of the control input for i th CAV, respectively. Similar meanings take effect on $\underline{\mathbf{z}}^i$ and $\bar{\mathbf{z}}^i$.

Moreover, the objective of this OCP is to follow the reference trajectories generated by an efficient sampling-based algorithm. For an individual vehicle, it can be expressed as

$$Q_i(\mathbf{Z}^i, \mathbf{U}^i) = \sum_{\tau=0}^T \|\mathbf{z}_\tau^i - \mathbf{z}_{\text{ref}, \tau}^i\|_{\mathbf{Q}}^2 + \sum_{\tau=0}^{T-1} \|\mathbf{u}_\tau^i\|_{\mathbf{R}}^2, \quad (5)$$

where the weighted matrices are $\mathbf{Q} = \text{diag}\{q_x, q_y, q_\theta, q_v\}$ and $\mathbf{R} = \text{diag}\{q_\delta, q_a\}$. The expected outcome of the optimization problem (4) is to cooperatively follow the reference states with different weights while complying with vehicle model and staying in the safe region \mathcal{S}_τ^i to avoid collisions with each other.

D. Inter-Vehicle Collision Avoidance of CAVs

Under connected conditions, assume each CAV can receive real-time information from its neighbors in \mathcal{N}^i in a certain range and collaborate to generate maneuvers that prevent collisions. Typically, vehicles are represented as two circles,

and the criterion for collision detection is the distance between each pair of circles. For instance, to construct the safe region \mathcal{S}_τ^i , if there are $|\mathcal{N}^i| = N^i$ CAVs around i th CAV, there would be $2^2 N^i$ pairs of constraints that need to be considered.

Alternatively, we can reduce the number of above constraints by modeling certain CAVs, such as a CAV with a lower order in a pair of CAVs, as ellipses [39], while representing the other CAV in the pair as double circles. This would decrease the constraints number by $2N^i$ for constructing the \mathcal{S}_τ^i . For a CAV pair (n^i and n^j) using the above description, we formulate the following constraints for inter-vehicle collision avoidance:

$$\begin{aligned}
 \frac{(\hat{x}_\tau^j - \hat{x}_\tau^{i,c})^2}{(a^j + r^i)^2} + \frac{(\hat{y}_\tau^j - \hat{y}_\tau^{i,c})^2}{(b^j + r^i)^2} &\geq 1, \\
 \forall c \in \mathcal{C}, j \in \mathcal{N}^i, i \in \mathcal{N}, \tau \in \mathcal{T},
 \end{aligned} \quad (6)$$

where \hat{x} and \hat{y} means the rotated position w.r.t. the $x' - y'$ coordinate parallel to the semi-major axis a of the ellipse (a -parallel coordinate) of (x, y) , $\mathcal{C} = \{0, 1\}$ denotes the front and rear circle of a CAV, $\mathcal{N}^i \in \mathbb{Z}_+^{\text{deg}(n^i)}$ denotes the index set of the neighbor CAVs within the communication range r_{tele}^i of the i th CAV. The discriminant (6) comes into effect for the following reason. In Fig. 2, we can observe that after applying rotation and translation transformations to align with the a -parallel coordinate system, the origin is the center of the CAV n^j and the x' -axis is parallel to the semi-major axis of the CAV n^j . Then we proceed to enlarge the ellipse by the radius of the circles r^i encapsulating the other CAV. Consequently, we utilize the coordinates of the circle centers in (6) to assess whether these centers fall within the enlarged ellipse. If this condition is met, it signifies a collision between the two CAVs. We will make the scaling transformation to make a more compact constraint form in Section IV-B.

For the coordinate transformation of the CAV's position from the global coordinate to the a -parallel coordinate, the following equation is given:

$$\hat{\mathbf{p}}_\tau^k = \begin{bmatrix} \cos \theta_\tau^j & \sin \theta_\tau^j \\ -\sin \theta_\tau^j & \cos \theta_\tau^j \end{bmatrix} \cdot \mathbf{p}_\tau^k = \mathbf{R}_\tau^j \cdot \mathbf{p}_\tau^k, \quad (7)$$

where $\hat{\mathbf{p}}_\tau^k = [\hat{x}_\tau^k, \hat{y}_\tau^k]^T$ is the position of the k th vehicle under the a -parallel coordinate, while \mathbf{p}_τ^k is the position under the

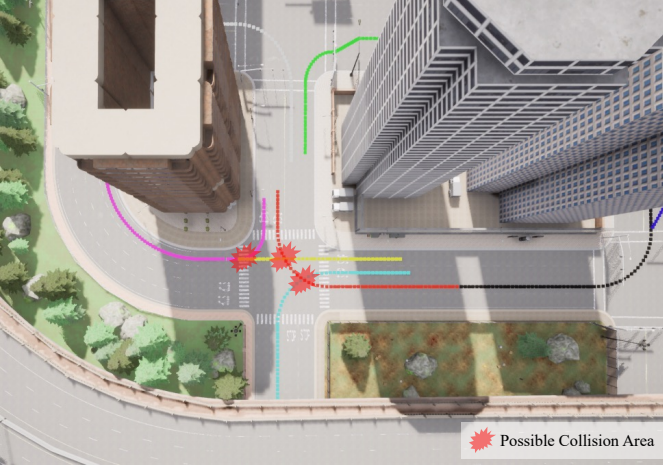


Fig. 3. Smoothed guidance trajectories for cooperative motion planning. We generate these trajectories by sampling the road topology information from the OpenDRIVE map. Each vehicle's trajectory is visually represented by dots of different colors. The plotted guidance trajectories unveil potential collision conflicts that may arise within the intersection area.

global $x - y$ coordinate in Fig. 2. Another notation R_τ^j is the transformation matrix to the a -paralleled coordinate. Besides, if given the center position \mathbf{p}_τ^i of the CAV n^i , the center positions of the front and rear circles are expressed as:

$$\mathbf{p}_\tau^{i,c} = \mathbf{p}_\tau^i \pm \begin{bmatrix} \cos \theta_\tau^i \\ \sin \theta_\tau^i \end{bmatrix} d^{i,c}. \quad (8)$$

Clearly, There are two circles $\mathbf{p}_\tau^{i,0}$ and $\mathbf{p}_\tau^{i,1}$ that need to be transformed. The centers of these circles can be transformed using (7), which involves replacing \mathbf{p}_τ^k with $\mathbf{p}_\tau^{i,c}$. With this, the transformed positions of the circles, $\hat{\mathbf{p}}_\tau^{i,0}$ and $\hat{\mathbf{p}}_\tau^{i,1}$, can be obtained. Additionally, the distance of the c th circle to the center of the i th CAV is denoted by $d^{i,c}$.

IV. COOPERATIVE MOTION PLANNING WITH LIMITED COMMUNICATION VIA IMPROVED CONSENSUS ADMM

A. Guidance Trajectory Generation and Dynamic Search

In the rough trajectory generation process, waypoints are sampled along the center line of lanes with equal intervals in the OpenDRIVE format map. As illustrated in Fig. 3, use the same approach in [33], for any starting point $\mathbf{x}^s = [p_x^s, p_y^s, \varphi^s]^\top$, A* search can be performed on the connectivity graph to obtain the shortest path leading to the target destination $\mathbf{x}^t = [p_x^t, p_y^t, \varphi^t]^\top$. Note that we use the Savitzky-Golay filter to improve the continuity and smoothness of the searched path, which makes the distribution of waypoints more even, especially around intersections, corners, and regions for lane changing.

Remark 1. For cooperative motion planning problems, the temporal trajectories of CAVs may not always be strictly followed due to the influence of surrounding vehicles' behavior. To address this, it becomes necessary to enable CAVs to automatically follow an appropriate waypoint based on their current state. One approach to achieving this is by searching for the nearest waypoint that the vehicle should follow.

After the global reference waypoints are obtained, the local reference waypoints can be determined utilizing a Nearest Neighbor Search mechanism for updating the reference trajectory of each CAV. Concretely, at each time step, each CAV searches for the nearest waypoint using a KD-tree formulated by the waypoints in its rough reference trajectory.

Remark 2. The utilization of the KD-tree data structure is shown to be highly efficient, particularly when dealing with a large number of waypoints. This guidance waypoint searching process minimally impacts the efficiency of the cooperative motion planning algorithm while offering a more robust and comfortable riding experience.

B. Convexification and Reformulation

In this section, we assume that all the CAVs are allocated to the same subgraph \mathcal{H} . To achieve fully decentralized motion planning for the CAVs efficiently, the objective function of the OCP should be convexified, and the constraints should be linearized [26]. In this paper, we transform the optimization variables from \mathbf{z}_τ^i and \mathbf{u}_τ^i to perturbed forms $\Delta \mathbf{z}_\tau^i$ and $\Delta \mathbf{u}_\tau^i$. Firstly, the vehicle model can be linearized by first-order Taylor expansion:

$$\Delta \mathbf{z}_{\tau+1}^i = \mathbf{A}_\tau^i \Delta \mathbf{z}_\tau^i + \mathbf{B}_\tau^i \Delta \mathbf{u}_\tau^i, \quad (9)$$

where $\mathbf{A}_\tau^i = \partial f(\mathbf{z}_\tau^i, \mathbf{u}_\tau^i) / \partial \mathbf{z}_\tau^i$, $\mathbf{B}_\tau^i = \partial f(\mathbf{z}_\tau^i, \mathbf{u}_\tau^i) / \partial \mathbf{u}_\tau^i$ are the partial derivatives of the vehicle model.

Secondly, the inter-vehicle collision avoidance constraints between pairs of vehicles can be rewritten and convexified as follows. We define the following function with perturbed variable vector $\Delta \bar{\mathbf{p}}_\tau^k = [\Delta \bar{x}_\tau^k, \Delta \bar{y}_\tau^k]^\top$ as the discriminant for inter-vehicle collision avoidance in the a -paralleled coordinate:

$$f_S(\mathbf{z}_\tau^j, \mathbf{z}_\tau^{i,c}) = \mathbf{k}_\tau^{ij} \Delta \bar{\mathbf{p}}_\tau^{ij} + \|\bar{\mathbf{p}}_\tau^{ij}\|_2 - d_{\text{safe}}, \quad (10)$$

$$\forall c \in \mathcal{C}, i \in \mathcal{N}^j, j \in \mathcal{N}^i, \tau \in \mathcal{T}^+,$$

where $\mathbf{k}_\tau^{ij} = \frac{\bar{\mathbf{p}}_\tau^{ij}}{\|\bar{\mathbf{p}}_\tau^{ij}\|}$ is a unit vector for projective transformation of the perturbed displacement to the direction from the i th CAV to the j th one, $d_{\text{safe}} \geq 1$ is the obstacle avoidance margin, $\mathcal{T}^+ = \{0, 1, \dots, T\}$, $\bar{\mathbf{p}}_\tau^{ij}$ is the relevant position of the pair of CAVs, and it can be calculated by:

$$\bar{\mathbf{p}}_\tau^{ij} = \mathbf{S}^{ij} \mathbf{R}_\tau^j (\mathbf{p}_\tau^{i,c} - \mathbf{p}_\tau^j), \quad (11)$$

where $\mathbf{S}^{ij} = \text{diag}\{\frac{1}{a^j + r^i}, \frac{1}{b^j + r^i}\}$. Given the state vectors \mathbf{z}_τ^j and \mathbf{z}_τ^i as the working points, the perturbed relevant position $\Delta \bar{\mathbf{p}}_\tau^{ij}$ can be calculated by:

$$\Delta \bar{\mathbf{p}}_\tau^{ij} = \frac{\partial \bar{\mathbf{p}}_\tau^{ij}}{\partial \mathbf{z}_\tau^j} \Delta \mathbf{z}_\tau^j + \frac{\partial \bar{\mathbf{p}}_\tau^{ij}}{\partial \mathbf{z}_\tau^i} \Delta \mathbf{z}_\tau^i. \quad (12)$$

Plugging (7), (8), and (11) to (12), the partial derivative of the CAV n^j at time step τ is

$$\begin{aligned} \frac{\partial \bar{\mathbf{p}}_\tau^{ij}}{\partial \mathbf{z}_\tau^j} &= \mathbf{S}^{ij} \frac{\partial \mathbf{R}_\tau^j \mathbf{p}_\tau^{i,c}}{\partial \mathbf{z}_\tau^j} + \mathbf{S}^{ij} \frac{\partial \mathbf{R}_\tau^j \mathbf{p}_\tau^j}{\partial \mathbf{z}_\tau^j} \\ &= \mathbf{S}^{ij} \left(\begin{bmatrix} 0 & 0 & -\sin \theta_\tau^j x_\tau^{i,c} + \cos \theta_\tau^j y_\tau^{i,c} & 0 \\ 0 & 0 & -\cos \theta_\tau^j x_\tau^{i,c} - \sin \theta_\tau^j y_\tau^{i,c} & 0 \end{bmatrix} \right. \\ &\quad \left. - \begin{bmatrix} \cos \theta_\tau^j & \sin \theta_\tau^j & -\sin \theta_\tau^j x_\tau^j + \cos \theta_\tau^j y_\tau^j & 0 \\ -\sin \theta_\tau^j & \cos \theta_\tau^j & -\cos \theta_\tau^j x_\tau^j - \sin \theta_\tau^j y_\tau^j & 0 \end{bmatrix} \right), \end{aligned}$$

while the partial derivative of the CAV n^i at time step τ is

$$\begin{aligned} \frac{\partial \bar{p}_\tau^{ij}}{\partial z_\tau^i} &= \mathbf{S}^{ij} \mathbf{R}_\tau^j \frac{\partial \mathbf{p}_\tau^{i,c}}{\partial z_\tau^i} \\ &= \mathbf{S}^{ij} \mathbf{R}_\tau^j \begin{bmatrix} 1 & 0 & \mp d^{i,c} \sin \theta_\tau^i & 0 \\ 0 & 1 & \pm d^{i,c} \cos \theta_\tau^i & 0 \end{bmatrix}, \end{aligned}$$

where for the front and rear circles of the i th CAV, the third column elements in the derivative matrices have opposite signs. The vehicle is in the safe set \mathcal{S}_τ if $f_S(\hat{\mathbf{p}}_\tau, \hat{\mathbf{p}}_\tau^{i,c}) \geq 0$. Therefore, with the new notation of

$$\mathbf{J}_{ic\tau}^j = \mathbf{k}_\tau^{ij} \mathbf{S}^{ij} \left(\frac{\partial \mathbf{R}_\tau^j \mathbf{p}_\tau^{i,c}}{\partial z_\tau^j} + \frac{\partial \mathbf{R}_\tau^j \mathbf{p}_\tau^j}{\partial z_\tau^j} \right), \quad (13)$$

$$\mathbf{J}_{j\tau}^{i,c} = \mathbf{k}_\tau^{ij} \mathbf{S}^{ij} \mathbf{R}_\tau^j \frac{\partial \mathbf{p}_\tau^{i,c}}{\partial z_\tau^i}, \quad (14)$$

the discriminant of the safety indicator is approximated as:

$$\|\mathbf{S}^{ij} \mathbf{R}_\tau^j (\mathbf{p}_\tau^{i,c} - \mathbf{p}_\tau^j)\|_2 + \mathbf{J}_{ic\tau}^j \Delta z_\tau^j + \mathbf{J}_{j\tau}^{i,c} \Delta z_\tau^i - d_{\text{safe}} \geq 0, \quad (15)$$

where $j \in \mathcal{N}^i$, $i \in \mathcal{N}^j$, $c \in \mathcal{C}$, and $\tau \in \mathcal{T}^+$.

Third, the vehicle state and control input constraints w.r.t the perturbed variables $\Delta \mathbf{z}$ and $\Delta \mathbf{u}$ can be written as:

$$\begin{aligned} \underline{z}^i - z_\tau^i &\leq \Delta z_\tau^i \leq \bar{z}^i - z_\tau^i, \\ \underline{u}^i - u_\tau^i &\leq \Delta u_\tau^i \leq \bar{u}^i - u_\tau^i. \end{aligned} \quad (16)$$

All the constraints of the original cooperative problem (4) are linearized and transformed by (9), (15), and (16).

Lastly, the quadratic objective function in (4) w.r.t the perturbed independent variables $\Delta \mathbf{z}_\tau^i$ can be derived by the second-order Taylor Expansion, which can be described as:

$$\begin{aligned} \bar{Q}_\tau^i(\Delta \mathbf{z}_\tau^i, \Delta \mathbf{u}_\tau^i) &\approx Q_\tau^i(z_\tau^i, \mathbf{u}_\tau^i) + \Delta \mathbf{u}_\tau^{i\top} Q_{\tau,u}^i + \Delta \mathbf{z}_\tau^{i\top} Q_{\tau,z}^i \\ &\quad + \frac{1}{2} \Delta \mathbf{u}_\tau^{i\top} Q_{\tau,uu}^i \Delta \mathbf{u}_\tau^i + \frac{1}{2} \Delta \mathbf{z}_\tau^{i\top} Q_{\tau,zz}^i \Delta \mathbf{z}_\tau^i, \end{aligned}$$

where $\tau \in \mathcal{T}$, $Q_\tau^i(\Delta \mathbf{z}_\tau^i, \Delta \mathbf{u}_\tau^i) = Q_\tau^i(z_\tau^i + \Delta \mathbf{z}_\tau^i, \mathbf{u}_\tau^i + \Delta \mathbf{u}_\tau^i)$. In addition, $Q_{\tau,u}^i$ and $Q_{\tau,z}^i$ are the partial derivatives of Q_τ^i w.r.t. \mathbf{u}_τ^i and z_τ^i , while $Q_{\tau,uu}^i$ and $Q_{\tau,zz}^i$ are the second-order partial derivatives of Q_τ^i w.r.t. \mathbf{u}_τ^i and z_τ^i . Note that the state vector and the control input vector are decoupled, hence the second-order mixed derivatives $Q_{\tau,uz}^i = Q_{\tau,zu}^i = \mathbf{0}$. With a similar definition of \bar{Q}_τ^i , the terminal cost is

$$\bar{Q}_T^i(\Delta \mathbf{z}_T^i) \approx Q_T^i(z_T^i) + \Delta \mathbf{z}_T^{i\top} Q_{T,z}^i + \frac{1}{2} \Delta \mathbf{z}_T^{i\top} Q_{T,zz}^i \Delta \mathbf{z}_T^i.$$

The following part reformulates the OCP as a consensus optimization problem with a standard consensus ADMM form [25]. To facilitate the description of the independent variables of the cooperative problem, define $\Delta \mathbf{Z}^i = [\Delta \mathbf{z}_0^{i\top}, \Delta \mathbf{u}_0^{i\top}, \dots, \Delta \mathbf{z}_T^{i\top}]^\top \in \mathbb{R}^{6T+4}$ as the concatenated vector of all the state vectors and control inputs corresponding to the i th CAV. Besides, define $\mathbf{L}_1^i = [Q_{0,z}^i, Q_{0,u}^i, \dots, Q_{T,z}^i] \in \mathbb{R}^{6T+4}$ as the column vector containing all the first-order Jacobians, and $\mathbf{L}_2^i = \text{blocdiag}\{Q_{0,zz}^i, Q_{0,uu}^i, \dots, Q_{T,zz}^i\} \in \mathbb{R}^{(6T+4) \times (6T+4)}$ as the block diagonal matrix of all second-order Hessians. Hence, the perturbed overall host cost is

$$\bar{F}^i(\Delta \mathbf{Z}^i) = \Delta \mathbf{Z}^{i\top} \mathbf{L}_1^i + \frac{1}{2} \Delta \mathbf{Z}^{i\top} \mathbf{L}_2^i \Delta \mathbf{Z}^i. \quad (17)$$

With a similar expression, the vehicle model (9) can be described by

$$(\mathbf{L}_3^i - \mathbf{L}_4^i) \Delta \mathbf{Z}^i = 0, \quad (18)$$

where $\mathbf{L}_3^i = \text{blocdiag}\{[\mathbf{A}_0^i \ \mathbf{B}_0^i], [\mathbf{A}_1^i \ \mathbf{B}_1^i], \dots, [\mathbf{A}_{T-2}^i \ \mathbf{B}_{T-2}^i], [\mathbf{A}_{T-1}^i \ \mathbf{B}_{T-1}^i \ \mathbf{0}^{4 \times 4}]\} \in \mathbb{R}^{(4T) \times (6T+4)}$ and $\mathbf{L}_4^i = \text{blocdiag}\{[\mathbf{0}^{4 \times 4} \ \mathbf{0}^{4 \times 2} \ \mathbf{I}^4], [\mathbf{0}^{4 \times 2} \ \mathbf{I}^4], \dots, [\mathbf{0}^{4 \times 2} \ \mathbf{I}^4]\} \in \mathbb{R}^{(4T) \times (6T+4)}$. Then, we define the solution set of the linearized vehicle model as

$$\mathcal{S}^D = \{\Delta \mathbf{Z}^i | (\mathbf{L}_3^i - \mathbf{L}_4^i) \Delta \mathbf{Z}^i = 0\}, \quad (19)$$

which is nonempty, closed, and convex. In conclusion, when combining the indicator function related to \mathcal{S}^D with the cost associated with the host, the resulting expression can be written as:

$$F^i(\Delta \mathbf{Z}^i) = \bar{F}^i(\Delta \mathbf{Z}^i) + \mathcal{I}_{\mathcal{S}^D}(\Delta \mathbf{Z}^i). \quad (20)$$

Afterward, we formulate the inter-vehicle collision avoidance constraints and vehicle physical constraints. We combine the inequality constraints into another indicator function $\mathcal{I}_{\mathcal{K}}$ corresponding to the feasible set of (15) and (16). For inter-vehicle collision avoidance constraints, the Jacobian matrices in (13) and (14) should be concatenated in the following order. For i th CAV, its concatenated Jacobian at time step τ is

$$\mathbf{J}_\tau^i = [\mathbf{a}_{jk}^\top]_{1 \leq j < k \leq N}^\top \in \mathbb{R}^{N(N-1) \times 4}, \quad (21)$$

where according to (13) and (14), \mathbf{a}_{jk} can be expressed as

$$\mathbf{a}_{jk} = \begin{cases} [\mathbf{J}_{k0\tau}^i; \mathbf{J}_{ki\tau}^i] & j = i \\ [\mathbf{J}_{j\tau}^{i,0}; \mathbf{J}_{j\tau}^{i,1}] & k = i \\ \mathbf{0}^{2 \times 4} & \text{otherwise.} \end{cases} \quad (22)$$

With the expression of the Jacobian \mathbf{J}_τ^i , we define $\hat{\mathbf{J}}^i = \text{blocdiag}\{[\mathbf{J}_0^i \ \mathbf{0}^{N(N-1) \times 2}], \dots, [\mathbf{J}_{T-1}^i \ \mathbf{0}^{N(N-1) \times 2}], \mathbf{J}_T^i\}$. Further, with a slight abuse of notation, we define the norm vector \mathbf{k}_τ constructed by $\|\mathbf{S}^{ij} \mathbf{R}_\tau^j (\mathbf{p}_\tau^{i,c} - \mathbf{p}_\tau^j)\|_2$ at time step τ with a similar modality of (21), which is

$$\mathbf{k}_\tau = [\|\mathbf{S}^{ij} \mathbf{R}_\tau^j (\mathbf{p}_\tau^{i,c} - \mathbf{p}_\tau^j)\|_2]_{1 \leq j < i \leq N} \in \mathbb{R}^{N \times (N-1)}, \quad (23)$$

where $c \in \mathcal{C}$. Concatenating \mathbf{k}_τ at all time steps, we define $\hat{\mathbf{k}} = [\mathbf{k}_\tau]_{\tau \in \mathcal{T}^+} \in \mathbb{R}^{N(N-1)(T+1)}$. Then, we rewrite the collision avoidance discriminant (15) of all the CAVs through the planning horizon as:

$$\hat{\mathbf{k}} + \sum_{i=1}^N \hat{\mathbf{J}}^i \Delta \mathbf{Z}^i - d_{\text{safe}}^{N(N-1)(T+1)} \succeq 0. \quad (24)$$

For the box constraints in (16), we define a new matrix $\bar{\mathbf{O}}^i$ step by step. We define a new variable $\Delta \mathbf{e}^i = [\Delta \hat{\mathbf{e}}^i, \Delta v_T^i]^\top \in \mathbb{R}^{3T+1}$ with the notation of $\Delta \hat{\mathbf{e}}^i = [[\Delta v_\tau^i, \Delta \delta_\tau^i, \Delta a_\tau^i]^\top]_{i \in \mathcal{T}}$, where $\Delta \mathbf{e}^i$ denotes the variables with box constraints in the dynamic system (2). Then $\Delta \mathbf{e}^i = \mathbf{O}^i \Delta \mathbf{Z}^i$, where

$$\mathbf{O}^i = \text{blocdiag}\{\underbrace{[\mathbf{0}^{3 \times 3}, \mathbf{I}^3]}_T, \dots, [\mathbf{0}^{1 \times 3}, 1]\} \in \mathbb{B}^{(3T+1) \times (6T+4)}.$$

To facilitate the form $\Delta \mathbf{e} = \sum_{i=1}^N \hat{\mathbf{O}}^i \Delta \mathbf{Z}^i$ required in the dual consensus ADMM algorithm [40], we further define

$$\hat{\mathbf{O}}^i = \underbrace{[\mathbf{0}^{(3T+1) \times (6T+4)}, \dots, \mathbf{O}^i, \mathbf{0}^{(3T+1) \times (6T+4)}, \dots]}_{i-1}, \underbrace{\quad}_{N-i}, \quad (25)$$

where $\hat{\mathbf{O}}^i \in \mathbb{B}^{(3T+1)N \times (6T+4)}$. Hence, the discriminant (16) for all the CAVs can be aggregated and rewritten as

$$\underline{\mathbf{E}} - \mathbf{E}_\tau \leq \sum_{i=1}^N \hat{\mathbf{O}}^i \Delta \mathbf{Z}^i \leq \overline{\mathbf{E}} - \mathbf{E}_\tau, \quad (26)$$

where $\mathbf{E}_\tau = [e^i]_{i \in \mathcal{N}}$, is the concatenated state and control input vectors of all the vehicles at time step τ . $\underline{\mathbf{E}}$ and $\overline{\mathbf{E}}$ denote the lower and upper bounds, respectively. With the notation $\mathbf{k} = [-\hat{\mathbf{k}} + \mathbf{d}_{\text{safe}}^{N(N-1)(T+1)}, \mathbf{0}^{(3T+1)N}] \in \mathbb{R}^{N(N-1)(T+1) + (3T+1)N}$, we formulate the second element of the unconstrained problem by the following two functions

$$G_1(\mathbf{M}_{g1}) = \mathcal{I}_{\mathcal{R}_+}(\mathbf{M}_{g1} - \mathbf{k}), \quad G_2(\mathbf{M}_{g2}) = \mathcal{I}_{\mathcal{S}^b}(\mathbf{M}_{g2}),$$

where the subscripts \mathcal{R}_+ denotes a positive semidefinite cone with a $N(N-1)(T+1)$ dimension and $\mathcal{S}^b = \{\mathbf{s} | \underline{\mathbf{E}} - \mathbf{E}_\tau \preceq \mathbf{s} \preceq \overline{\mathbf{E}} - \mathbf{E}_\tau\}$ denotes a continuous convex set with a $(3T+1)N$ dimension, respectively. The independent variables are

$$\mathbf{M}_{g1} = \sum_{i=1}^N (\hat{\mathbf{J}}^i \Delta \mathbf{Z}^i), \quad \mathbf{M}_{g2} = \sum_{i=1}^N \hat{\mathbf{O}}^i \Delta \mathbf{Z}^i.$$

Concatenating $\hat{\mathbf{J}}^i$ with the upper and lower bound constraints in (25) as $\mathbf{J}^i = [\hat{\mathbf{J}}^i; \hat{\mathbf{O}}^i]$, we define the concatenated function

$$G(\mathbf{M}) = G(\mathbf{M}_{[1]}; \mathbf{M}_{[1]}) = \mathcal{I}_{\mathcal{K}} \left(\sum_{i=1}^N \mathbf{J}^i \Delta \mathbf{Z}^i - \mathbf{k} \right),$$

where $\mathbf{M} = \sum_{i=1}^N \mathbf{J}^i \Delta \mathbf{Z}^i$ and $\mathcal{K} = \{(\mathbf{a}; \mathbf{b}) | \mathbf{a} \in \mathcal{R}_+, \mathbf{b} \in \mathcal{S}^b\}$ is the Cartesian product of the two sets \mathcal{R}_+ and \mathcal{S}^b . Note that $G(\cdot)$, the sum of two convex functions $G_1(\cdot)$ and $G_2(\cdot)$, is still convex. At this stage, by including $G(\cdot)$ in the overall cost incurred by $F(\cdot)$, with a new notation of $\mathbf{k}^i = \mathbf{k}/N$, the unconstrained convex optimization problem is given by:

$$\min_{\Delta \mathbf{Z}^i} \sum_{i=1}^N F^i(\Delta \mathbf{Z}^i) + \mathcal{I}_{\mathcal{K}} \left(\sum_{i=1}^N (\mathbf{J}^i \Delta \mathbf{Z}^i - \mathbf{k}^i) \right). \quad (27)$$

C. Improved Consensus ADMM for Cooperative Motion Planning with Limited Communication Range

In this part, we leverage a parallel optimization framework based on dual consensus ADMM and improve its computational efficiency. For completeness, we restate the preliminaries of dual consensus ADMM [25], as also summarized in Algorithm 1. We add the relax variable \mathbf{h} and adapt the dual formulation of the problem (27) as:

$$\begin{aligned} \min_{\Delta \mathbf{Z}^1, \dots, \Delta \mathbf{Z}^N} & \sum_{i=1}^N F^i(\Delta \mathbf{Z}^i) + \mathcal{I}_{\mathcal{K}}(\mathbf{h}) \\ \text{s.t.} & \sum_{i=1}^N (\mathbf{J}^i \Delta \mathbf{Z}^i - \mathbf{k}^i) = \mathbf{h}. \end{aligned} \quad (28)$$

Algorithm 1 Dual Consensus ADMM [40]

- 1: **choose** $\sigma, \rho > 0$
 - 2: **initialize** for all $i \in \mathcal{N}$: $p^{i,0} = y^{i,0} = x^{i,0} = s^{i,0} = 0$
 - 3: **repeat**: for all $i \in \mathcal{N}$
 - 4: Broadcast $y^{i,k}$ to the vehicles in \mathcal{N}^i
 - 5: $p^{i,k+1} = p^{i,k} + \rho \sum_{j \in \mathcal{N}^i} (y^{i,k} - y^{j,k})$
 - 6: $s^{i,k+1} = s^{i,k} + \sigma (y^{i,k} - x^{i,k})$
 - 7: $r^{i,k+1} = \sigma x^{i,k} + \rho \sum_{j \in \mathcal{N}^i} (y^{i,k} + y^{j,k}) - (k^i + p^{i,k+1} + s^{i,k+1})$
 - 8: $z^{i,k+1} = \arg \min \{ F^i(z^i) + \gamma \|J^i z^i + r^{i,k+1}\|^2 \}$
 - 9: $y^{i,k+1} = 2\gamma (J^i z^{i,k+1} + r^{i,k+1})$
 - 10: $x^{i,k+1} = \Pi_{\mathcal{K}^\circ} (\frac{1}{\sigma} s^{i,k+1} + y^{i,k+1})$
 - 11: $k = k + 1$
 - 12: **until** termination criterion is satisfied
-

In this problem, Slater's condition holds under affine constraints, which ensures the strong duality property. The Lagrangian of (28) is given by:

$$\begin{aligned} \mathcal{L}(\Delta \mathbf{Z}, \mathbf{h}, \mathbf{y}) &= \sum_{i=1}^N F^i(\Delta \mathbf{Z}^i) + \mathcal{I}_{\mathcal{K}}(\mathbf{h}) \\ &+ \mathbf{y}^\top \left(\sum_{i=1}^N (\mathbf{J}^i \Delta \mathbf{Z}^i - \mathbf{k}^i) - \mathbf{h} \right), \end{aligned} \quad (29)$$

where $\mathbf{y} \in \mathbb{R}^{N(N-1)(T+1) + (3T+1)N}$ represents the dual variable relating to the inter-vehicle collision avoidance constraints and box constraints from the vehicle physics. The Lagrange dual function can be expressed as:

$$\begin{aligned} h(\mathbf{y}) &= \inf_{\Delta \mathbf{Z}, \mathbf{h}} \mathcal{L}(\Delta \mathbf{Z}, \mathbf{h}, \mathbf{y}) \\ &= - \sum_{i=1}^N (F^{i*}(-\mathbf{J}^{i\top} \mathbf{y}) + \mathcal{I}_{\mathcal{K}^\circ}(\mathbf{y}) + \mathbf{y}^\top \mathbf{k}^i). \end{aligned} \quad (30)$$

Note that F^{i*} represents the conjugates of F^i and $\mathcal{K}^\circ = \{\mathbf{y} \in \mathbb{R}^{N(N-1)(T+1) + (3T+1)N} | \sup_{\mathbf{h} \in \mathcal{K}} \mathbf{y}^\top \mathbf{h} \leq 0\}$ is the polar cone of the convex cone \mathcal{K} . The problem of the Lagrange dual problem, i.e.,

$$\max_{\mathbf{y}} h(\mathbf{y}) = \max_{\mathbf{y}} - \sum_{i=1}^N (F^{i*}(-\mathbf{J}^{i\top} \mathbf{y}) + \mathcal{I}_{\mathcal{K}^\circ}(\mathbf{y}) + \mathbf{y}^\top \mathbf{k}^i),$$

can be treated as a consensus optimization problem that is decomposed. In this problem, all vehicles collaborate to collectively reach a decision on a shared optimization variable, denoted as \mathbf{y} . Consequently, the consensus ADMM Algorithm 1 can be applied.

Leveraging the methodological results in [26], we are able to get the analytical expressions of the column vectors $\mathbf{p}, \mathbf{s}, \mathbf{r}, \mathbf{y}, \mathbf{x} \in \mathbb{R}^{N(N-1)(T+1) + (3T+1)N}$ shown in Algorithm 1. The improved consensus ADMM for cooperative motion planning problem contains the following two steps:

1) *Dual Update*: The decentralized local problems corresponding to each CAV achieves consensus by dual update process. In Algorithm 1, we define $\gamma = \frac{1}{2(\sigma + 2\rho|n^i|)}$. Steps 5-7 and 9-10 are used to update the dual variables. Note that in Step 5 and Step 7, the i th CAV only processes the Jacobian

Matrices related to its own neighbors in \mathcal{N}^i . All steps are straightforward, except for Step 10. Based on the Moreau decomposition [41], the projection operator can be expressed as $\Pi_{\mathcal{K}^c}(\mathbf{a}) = \mathbf{a} - \Pi_{\mathcal{K}}(\mathbf{a})$. Therefore, Step 10 can be rewritten as

$$\mathbf{x}^{i,k+1} = \frac{1}{\sigma} \mathbf{s}^{i,k+1} + \mathbf{y}^{i,k+1} - \boldsymbol{\lambda}^{i,k+1}, \quad (31)$$

where $\boldsymbol{\lambda}^{i,k+1}$ is an intermediate variable calculated by:

$$\begin{aligned} \boldsymbol{\lambda}^{i,k+1} &= \Pi_{\mathcal{K}} \left(\frac{1}{\sigma} \mathbf{s}^{i,k+1} + \mathbf{y}^{i,k+1} \right) \\ &= \operatorname{argmin}_{\mathbf{q} \in \mathcal{K}} \left\| \mathbf{y}^{i,k+1} + \frac{1}{\sigma} \mathbf{s}^{i,k+1} - \mathbf{q} \right\| \\ &= \max \left\{ \boldsymbol{\Lambda}, \min \left\{ \boldsymbol{\Gamma}, \mathbf{y}^{i,k+1} + \frac{1}{\sigma} \mathbf{s}^{i,k+1} \right\} \right\}, \end{aligned} \quad (32)$$

where k means the number of the ADMM iteration. Based on the definition of the Cartesian product \mathcal{K} , we denote the element-wise lower bound and upper bound as $\boldsymbol{\Lambda} = [\mathbf{0}^{N(N-1)(T+1)}, \underline{\mathbf{E}}] + \boldsymbol{\epsilon}$ and $\boldsymbol{\Gamma} = [\infty^{N(N-1)(T+1)}, \overline{\mathbf{E}}] - \boldsymbol{\epsilon}$, respectively. Here, $\boldsymbol{\epsilon} = [\epsilon]^{N(N-1)(T+1)+(3T+1)N}$ is a vector filled with a small non-negative number ϵ to push $\mathbf{x}^{i,k+1}$ away from the boundary into the feasible region, ensuring strict satisfaction of constraints in the original problem.

Remark 3. Due to the inherent decoupled nature of this optimization problem with respect to each element of \mathbf{x} , the solution can be easily obtained through element-wise maximization and minimization as described in (32).

2) *Primal Update:* Note that Step 8 of Algorithm 1 executes the primal update to explore the optimal states and control inputs for the i th CAV. The primal variable $z^{i,k+1} = \boldsymbol{\Delta} \mathbf{Z}^{i,k+1}$ denotes the augmented state of the i th CAV at the $(k+1)$ th ADMM iteration. It can be updated by solving a standard LQR problem:

$$\begin{aligned} \min_{\boldsymbol{\Delta} \mathbf{Z}^i} & \boldsymbol{\Delta} \mathbf{Z}^{i\top} \mathbf{L}_1^i + \frac{1}{2} \boldsymbol{\Delta} \mathbf{Z}^{i\top} \mathbf{L}_2^i \boldsymbol{\Delta} \mathbf{Z}^i + 2\mathbf{r}^{i,k+1\top} \mathbf{J}^i \boldsymbol{\Delta} \mathbf{Z}^i \\ & + \frac{1}{\sigma + 2\rho|n^i|} \boldsymbol{\Delta} \mathbf{Z}^{i\top} \mathbf{J}^{i\top} \mathbf{J}^i \boldsymbol{\Delta} \mathbf{Z}^i \\ \text{s.t.} & (\mathbf{L}_3^i - \mathbf{L}_4^i) \boldsymbol{\Delta} \mathbf{Z}^i = \mathbf{0}. \end{aligned} \quad (33)$$

It is worth noting that all terms of the objective function in (33) are quadratic, and the constraint for the vehicle model is linear. In this sense, the problem can be effectively solved using dynamic programming. Besides, the problem solely involves state variables and control inputs that are specific to a single CAV. Consequently, the problem described by (33) for different CAVs can be concurrently solved in a parallel manner.

Assumption 1. The maximum iterations for both the outer and inner loops in Algorithm 1 are fixed and the planning horizon in each iteration is constant.

Remark 4. Although the LQR problem can be efficiently solved using the algebraic Riccati equation, it still requires dealing with the high-dimensional Jacobian matrix \mathbf{J} to obtain its inverse matrix. This process can be time-consuming, especially for large-scale cooperative motion planning problems.

With Assumption 1, if all the CAVs in \mathcal{H} are fully connected, the complexity of the Algorithm 1 is $\mathcal{O}(N^3)$, due to Step 5 and Step 7.

It is evident that the dual variables $\mathbf{p}, \mathbf{s}, \mathbf{r}, \mathbf{y}, \mathbf{x} \in \mathbb{R}^{N(N-1)(T+1)+(3T+1)N}$ are constructed corresponding to the inter-vehicle collision avoidance constraints $[\cdot]_{[1]}$ with a dimension of $N(N-1)(T+1)$ and the box constraints $[\cdot]_{[2]}$ with a dimension of $(3T+1)N$. Therefore, separate treatments are logical for these variable sets.

With the limited communication condition, $[\cdot]_{[1]}^i$ is calculated with the information from \mathcal{N}^i . In other words, the communication range limits the number of the non-zero Jacobian matrices for the inter-vehicle collision avoidance from $N(N-1)(T+1)$ to $N^i(N-1)(T+1)$, while the rest jacobian matrices are filled with $\mathbf{0}$. The number of terms to be summed in Step 5 and Step 7 are converted from N to N^i as well. Assuming N^i is a limited number, we derive the conclusion that the complexity of the calculation of $[\cdot]_{[1]}$ is decreased from $\mathcal{O}(N^3)$ to $\mathcal{O}(N)$ compared to the dual consensus ADMM algorithm assuming the fully connected topology network between CAVs [26].

On the other hand, $[\cdot]_{[2]}$ has redundant variables associated with other CAVs. We define $[\cdot]_{[2,i]} \in \mathbb{R}^{3T+1}$ as the $((i-1)(3T+1)+1)$ to $i(3T+1)$ rows of $[\cdot]_{[2]}$ pertaining to the box constraints. Based on the sparsity of $\hat{\mathbf{O}}^i$, we can reduce computational complexity by eliminating redundant entities except \mathbf{O}^i for $[\cdot]_{[2,i]}^i$. Assume $i \in \mathcal{N}^v$, as outlined in Algorithm 1, the dual variables for the v th CAV w.r.t. the i th CAV are iteratively updated using the following equations:

$$\mathbf{p}_{[2,i]}^{v,k+1} = \mathbf{p}_{[2,i]}^{v,k} + \rho \sum_{j \in \mathcal{N}^v} \left(\mathbf{y}_{[2,i]}^{v,k} - \mathbf{y}_{[2,i]}^{j,k} \right), \quad (34a)$$

$$\mathbf{s}_{[2,i]}^{v,k+1} = \mathbf{s}_{[2,i]}^{v,k} + \sigma \left(\mathbf{y}_{[2,i]}^{v,k} - \mathbf{x}_{[2,i]}^{v,k} \right), \quad (34b)$$

$$\begin{aligned} \mathbf{r}_{[2,i]}^{v,k+1} &= \sigma \mathbf{x}_{[2,i]}^{v,k} + \rho \sum_{j \in \mathcal{N}^v} \left(\mathbf{y}_{[2,i]}^{v,k} + \mathbf{y}_{[2,i]}^{j,k} \right) \\ &\quad - \left(\mathbf{k}_{[2,i]}^v + \mathbf{p}_{[2,i]}^{v,k+1} + \mathbf{s}_{[2,i]}^{v,k+1} \right), \end{aligned} \quad (34c)$$

$$\mathbf{y}_{[2,i]}^{v,k+1} = \begin{cases} 2\gamma \left(\mathbf{O}^i \boldsymbol{\Delta} \mathbf{Z}^{i,k+1} + \mathbf{r}_{[2,i]}^{i,k+1} \right) & v = i \\ 2\gamma \mathbf{r}_{[2,i]}^{v,k+1} & v \neq i, \end{cases} \quad (34d)$$

$$\mathbf{x}_{[2,i]}^{v,k+1} = \Pi_{\mathcal{S}^{u\circ}} \left(\frac{1}{\sigma} \mathbf{s}_{[2,i]}^{v,k+1} + \mathbf{y}_{[2,i]}^{v,k+1} \right), \quad (34e)$$

Theorem 1. Given that the dual variables of the CAVs are initialized by same values, for the elements of dual variables with $\forall j \neq i, \forall v \neq i, \boldsymbol{\alpha}_{[2,i]}^{j,k} = \boldsymbol{\alpha}_{[2,i]}^{v,k} = \boldsymbol{\alpha}_{[2,i]}^k, \boldsymbol{\alpha} \in \{\mathbf{p}, \mathbf{s}, \mathbf{r}, \mathbf{y}, \mathbf{x}\}, \forall k \in \mathcal{K}_{\text{iter}}$ holds.

Proof. Denote the statement of

$$P(m) : \boldsymbol{\alpha}_{[2,i]}^{j,m} = \boldsymbol{\alpha}_{[2,i]}^{v,m}, \boldsymbol{\alpha} \in \{\mathbf{p}, \mathbf{s}, \mathbf{r}, \mathbf{y}, \mathbf{x}\},$$

and the proof is given by induction on m .

Base case: With the same initialization of the dual variables, we have $\boldsymbol{\alpha}_{[2,i]}^{j,0} = \boldsymbol{\alpha}_{[2,i]}^{v,0} = \boldsymbol{\alpha}_{[2,i]}^0, \boldsymbol{\alpha} \in \{\mathbf{p}, \mathbf{s}, \mathbf{r}, \mathbf{y}, \mathbf{x}\}$, so $P(0)$ is clearly true.

Induction step: Assume the induction hypothesis that $\forall j \neq i, [\cdot]_{2,i}^{j,k} = [\cdot]_{2,i}^k$ holds, meaning $P(k)$ is true. According to (34), for the second term of the equations (34a) and (34c), because $\mathbf{y}_{[2,i]}^{v,k} = \mathbf{y}_{[2,i]}^{j,k} = \mathbf{y}_{[2,i]}^k, j \neq i, k \neq i$, we have:

$$\sum_{j \in \mathcal{N}^v} \left(\mathbf{y}_{[2,i]}^{v,k} - \mathbf{y}_{[2,i]}^{j,k} \right) = \mathbf{y}_{[2,i]}^k - \mathbf{y}_{[2,i]}^{i,k}, \quad (35)$$

$$\sum_{j \in \mathcal{N}^v} \left(\mathbf{y}_{[2,i]}^{v,k} + \mathbf{y}_{[2,i]}^{j,k} \right) = (2|n^v| - 1)\mathbf{y}_{[2,i]}^k + \rho\mathbf{y}_{[2,i]}^{i,k}. \quad (36)$$

Plug (35) and (36) to (34) under the case of $v \neq i$, the following equation holds:

$$\mathbf{p}_{[2,i]}^{v,k+1} = \mathbf{p}_{[2,i]}^k + \rho \left(\mathbf{y}_{[2,i]}^k - \mathbf{y}_{[2,i]}^{i,k} \right) = \mathbf{p}_{[2,i]}^{k+1}, \quad (37a)$$

$$\mathbf{s}_{[2,i]}^{v,k+1} = \mathbf{s}_{[2,i]}^k + \sigma \left(\mathbf{y}_{[2,i]}^k - \mathbf{x}_{[2,i]}^k \right) = \mathbf{s}_{[2,i]}^{k+1}, \quad (37b)$$

$$\begin{aligned} \mathbf{r}_{[2,i]}^{v,k+1} &= \sigma \mathbf{x}_{[2,i]}^k + \rho(2|n^v| - 1)\mathbf{y}_{[2,i]}^k + \rho\mathbf{y}_{[2,i]}^{i,k} \\ &\quad - (\mathbf{k}_{[2,i]}^{k+1} + \mathbf{p}_{[2,i]}^{k+1} + \mathbf{s}_{[2,i]}^{k+1}) = \mathbf{r}_{[2,i]}^{k+1}, \end{aligned} \quad (37c)$$

$$\mathbf{y}_{[2,i]}^{v,k+1} = 2\gamma \mathbf{r}_{[2,i]}^{k+1} = \mathbf{y}_{[2,i]}^{k+1}, \quad (37d)$$

$$\mathbf{x}_{[2,i]}^{v,k+1} = \Pi_{S^{b_0}} \left(\frac{1}{\sigma} \left(\mathbf{s}_{[2,i]}^{k+1} + \mathbf{y}_{[2,i]}^{k+1} \right) \right) = \mathbf{x}_{[2,i]}^{k+1}, \quad (37e)$$

which means the statement $P(k+1)$ also holds, establishing the induction step from $P(k)$ to $P(k+1)$. Since both the *base case* and the *induction step* have been proved as true, $P(m)$ holds for every $m \in \mathcal{K}_{\text{iter}}$. This completes the proof of Theorem 1. \square

Therefore, the dual update with $v \neq i$ can be completed by (37). Besides, according to (34) under the case of $v = i$, with Theorem 1, the dual update of $\alpha_{2,i}^{i,k+1}$ can be simplified as:

$$\mathbf{p}_{[2,i]}^{i,k+1} = \mathbf{p}_{[2,i]}^{i,k} + \rho(N-1) \left(\mathbf{y}_{[2,i]}^{i,k} - \mathbf{y}_{[2,i]}^k \right), \quad (38a)$$

$$\mathbf{s}_{[2,i]}^{i,k+1} = \mathbf{s}_{[2,i]}^{i,k} + \sigma \left(\mathbf{y}_{[2,i]}^{i,k} - \mathbf{x}_{[2,i]}^k \right), \quad (38b)$$

$$\begin{aligned} \mathbf{r}_{[2,i]}^{i,k+1} &= \sigma \mathbf{x}_{[2,i]}^{i,k} + \rho(N-1) \left(\mathbf{y}_{[2,i]}^{i,k} + \mathbf{y}_{[2,i]}^k \right) \\ &\quad - (\mathbf{k}_{[2,i]}^{i,k+1} + \mathbf{p}_{[2,i]}^{i,k+1} + \mathbf{s}_{[2,i]}^{i,k+1}), \end{aligned} \quad (38c)$$

$$\mathbf{y}_{[2,i]}^{i,k+1} = 2\gamma \left(\mathbf{O}^i \Delta \mathbf{Z}^i \mathbf{r}_{[2,i]}^{i,k+1} + \mathbf{r}_{[2,i]}^{i,k+1} \right), \quad (38d)$$

$$\mathbf{x}_{[2,i]}^{i,k+1} = \Pi_{S^{b_0}} \left(\frac{1}{\sigma} \left(\mathbf{s}_{[2,i]}^{i,k+1} + \mathbf{y}_{[2,i]}^{i,k+1} \right) \right). \quad (38e)$$

Remark 5. Combining (37) and (38), the decoupled ADMM iteration of variables corresponding to the box constraints of vehicle i is completed. Therefore, compared to (34), the computational complexity is reduced obviously from $\mathcal{O}(N^i)$ to $\mathcal{O}(1)$, which improves the computational efficiency but does not affect the optimization performance.

In summary, combining the solving process of $[\cdot]_{[1]}$ and $[\cdot]_{[2]}$, an improved decentralized cooperative motion planning algorithm with a computation complexity of $\mathcal{O}(N)$ is provided. As demonstrated in Algorithm 2, it starts by initializing the dual variables and choosing values for hyper-parameters. It then enters a loop where it sends and receives information among the CAVs in each \mathcal{N}^i . It computes the augmented

Algorithm 2 Improved Consensus ADMM for Cooperative Motion Planning Within One Subgraph $\mathcal{H}(\mathcal{N}, \mathcal{E}_h)$

- 1: **initialize** $\{x_\tau^i, u_\tau^i\}_{\tau=0}^T, \{p^{i,0}, y^{i,0}, z^{i,0}, s^{i,0}\}, \forall i \in \mathcal{N}$
 - 2: **choose** $\sigma, \rho > 0$
 - 3: **repeat**:
 - 4: Send $\{z_\tau^i\}_{\tau=1}^T$, receive $\{z_\tau^j\}_{\tau=1}^T$ from $j \in \mathcal{N}^i$
 - 5: Compute $k^i, J^i, \{A_\tau^i\}_{\tau=0}^{T-1}, \{B_\tau^i\}_{\tau=0}^{T-1}$
 - 6: **reset** $p^{i,0} = s^{i,0} = 0, y^{i,0} = y^{\text{last}}, x^{i,0} = x^{\text{last}}$
 - 7: **reset** $y_{[2]}^{i,0} = x_{[2]}^{i,0} = 0$
 - 8: **repeat**: for all $i \in \mathcal{N}$
 - 9: Send $y^{i,k}$, receive $y^{j,k}$ from $j \in \mathcal{N}^i$
 - 10: Steps 4-7 of Algorithm 1 for $[\cdot]_{[1]}^{i,k}$
 - 11: Perform (38a-38c) for $\alpha_{[2,i]}^{i,k}, \alpha \in \{p, s, r\}$
 - 12: Perform (37a-37c) for $\alpha_{[2,j]}^{i,k}, \alpha \in \{p, s, r\}, j \in \mathcal{N}^i$
 - 13: Compute $z^{i,k+1}$ by solving LQR problem (33)
 - 14: $y_{[1]}^{i,k+1} = 2\gamma \left(\hat{J}^i z_{[1]}^{i,k+1} + r_{[1]}^{i,k+1} \right)$
 - 15: $x_{[1]}^{i,k+1} = \Pi_{\mathcal{R}_+^o} \left(\frac{1}{\sigma} s_{[1]}^{i,k+1} + y_{[1]}^{i,k+1} \right)$
 - 16: Perform (38d-38e) for $\alpha_{[2,i]}^{i,k}, \alpha \in \{y, x\}$
 - 17: Perform (37d-37e) for $\alpha_{[2,j]}^{i,k}, \alpha \in \{y, x\}, j \in \mathcal{N}^i$
 - 18: $k = k + 1$
 - 19: **until** number of iteration steps exceeds k_{max}
 - 20: Update $\{z_\tau^i, u_\tau^i\}_{\tau=0}^T$
 - 21: **until** termination criterion is satisfied
-

variables based on the received neighbor information and performs computations for each time step τ . Inside the loop, it also performs additional computations and updates the primal variables until a termination criterion is satisfied. The inner loop continues to iterate until a maximum number of steps is reached. Finally, it updates the state vectors and control inputs along the whole planning horizon until the termination criterion of the outer loop is satisfied.

V. COOPERATIVE MOTION PLANNING FRAMEWORK FOR LARGE-SCALE CAVS

This section focuses on improving the practicality of the proposed algorithm toward cooperative motion planning with large-scale CAVs under a locally connected topology network. We leverage graph evolution and receding horizon strategies to achieve this objective.

A. Graph Evolution based on Manhattan Distance

To enable efficient decentralized cooperative motion planning for CAVs, a graph evolution strategy is presented incorporating node distribution algorithm and edge construction rules. The node distribution mechanism is demonstrated in Algorithm 3. Leveraging the notations in Section III-A, each node n^i is distributed into a subset of nodes $\mathcal{N}(\mathcal{H})$ from $\mathcal{V}(\mathcal{G})$, which belong to two graphs $\mathcal{H}(\mathcal{N}, \mathcal{E}_h)$ and $\mathcal{G}(\mathcal{V}, \mathcal{E})$, respectively. Their relationship can be described as:

$$\mathcal{H}(\mathcal{N}, \mathcal{E}_h) \subseteq \mathcal{G}(\mathcal{V}, \mathcal{E}). \quad (39)$$

The node distribution algorithm aims to establish the communication and collaboration among CAVs with certain discrimination rules, referred to as the threshold distance $d_{\text{safe}}^{i,j}$. To

Algorithm 3 Graph Evolution for CAVs

```

1: input: current positions  $p_{T_e}^i, i \in \mathcal{V}$ 
2: initialize: distance matrix  $D = [d^{i,j}], i, j \in \mathcal{V}$ 
3: reset: threshold distance  $d_{\text{safe}}^{i,j} = \infty$ 
4: if  $\Delta\theta < 45^\circ$  then
5:    $d_{\text{safe}}^{i,j} = T_s \cdot \max\{v_{\text{ref}}^i, v_{\text{ref}}^j\}$ 
6: else
7:    $d_{\text{safe}}^{i,j} = T_s \cdot (v_{\text{ref}}^i + v_{\text{ref}}^j)$ 
8: end if
9: build: adjacency matrix  $A_G$  with condition  $d^{i,j} < d_{\text{safe}}^{i,j}$ 
10: initialize: subgraphs list, visited list
11: for  $i$  in range (len( $D[0]$ )) do
12:   if visited[ $i$ ] is 0 then
13:     Create subgraph with  $i$ 
14:     Mark  $i$  as visited
15:     Initialize queue with  $i$ 
16:     while queue do
17:       Get node and neighbors from queue
18:       for neighbor in neighbors do
19:         if visited[neighbor] is 0 then
20:           Add neighbor to subgraph and queue
21:           Mark neighbor as visited
22:         end if
23:       end for
24:     end while
25:     Perform (43) to create the edge set  $\mathcal{E}_h$ 
26:     Add subgraph  $\mathcal{H}$  to subgraphs list
27:   end if
28: end for

```

divide the graph into as many subgraphs as possible under the inter-subgraph safety guarantee for the node distribution strategy, we propose a *safe distance* by the following conditional Manhattan distance:

$$d_{\text{safe}}^{i,j} = \begin{cases} T_s \cdot \max\{v_{\text{ref}}^i, v_{\text{ref}}^j\}, & \Delta\theta < \frac{\pi}{4} \\ T_s \cdot (v_{\text{ref}}^i + v_{\text{ref}}^j), & \text{otherwise.} \end{cases} \quad (40)$$

Vehicles with a Manhattan distance $d^{i,j} = \|\mathbf{p}^i - \mathbf{p}^j\|_1$ larger than the safe distance have no potential to collide with each other, which is explained by the following statements.

If $\Delta\theta < \frac{\pi}{4}$, the two CAVs appear to be driving in the same direction. In this case, the situation of the CAVs can be treated as a *Pursuit Problem*, where the relative velocity $\Delta v^{ij} = v^i - v^j < \max\{v^i, v^j\}$. Therefore, the relative displacement of the CAVs can be expressed as

$$\Delta d^{ij} = T_s \cdot \Delta v^{ij} < T_s \cdot \max\{v^i, v^j\}. \quad (41)$$

If $\Delta\theta \geq \frac{\pi}{4}$, the two CAVs are either *driving vertically* or *toward each other*. In the sub-case of *driving vertically*, a necessary and insufficient condition for the possibility of collision is given by *Condition 1*:

- $v_{\text{ref}}^i \times T_s \geq \Delta x_{\tau}^{ij}$ and $v_{\text{ref}}^j \times T_s \geq \Delta y_{\tau}^{ij}$, or
- $v_{\text{ref}}^j \times T_s \geq \Delta x_{\tau}^{ij}$ and $v_{\text{ref}}^i \times T_s \geq \Delta y_{\tau}^{ij}$

For *Condition 1*, an equivalent necessary and insufficient condition is listed as *Condition 2*:

- $v_{\text{ref}}^i \times T_s + v_{\text{ref}}^j \times T_s \geq \Delta x_{\tau}^{ij} + \Delta y_{\tau}^{ij} = \|\mathbf{p}^i - \mathbf{p}^j\|_1$

Hence, *Condition 2* is also a necessary and insufficient condition for collision avoidance. In the sub-case of *driving toward each other*, the situation of the CAVs can be treated as an Encounter Problem, where the relative velocity $\Delta v^{ij} \leq v_{\text{ref}}^i + v_{\text{ref}}^j$. Therefore, the relative displacement of the CAVs can be expressed as $\Delta d^{ij} = \Delta v^{ij} \times T_s \leq (v_{\text{ref}}^i + v_{\text{ref}}^j) \times T_s$. If $\Delta d^{ij} \leq \|(x_{\tau}^i, y_{\tau}^i) - (x_{\tau}^j, y_{\tau}^j)\|_1$, there is no possibility of encountering with a time horizon T_s , which means

$$\|(x_{\tau}^i, y_{\tau}^i) - (x_{\tau}^j, y_{\tau}^j)\|_1 > (v_{\text{ref}}^i + v_{\text{ref}}^j) \times T_s. \quad (42)$$

At this stage, all the cases are discussed the safety guarantee of conditional Manhattan distance is proved completely.

Remark 6. In urban traffic systems, roads are typically vertically staggered, and vehicles navigate based on the topology of the road network. Hence, we motivate the use of Manhattan distance to measure the safe range between CAVs. Each CAV has a target velocity, which is generally maintained for extended periods. Therefore, the product of the target velocity and the planning horizon can serve as a criterion for establishing a safety distance between any pair of CAVs.

As shown in Algorithm 3, a distance matrix D is firstly initialized to store the pairwise conditional Manhattan distances between $n^i \in \mathcal{V}$. The adjacency matrix A_G is then constructed based on an element-wise comparison of the distance i.e., $(n^i, n^j) = d^{i,j} < d_{\text{safe}}^{i,j}$. Hence, A_G represents the connectivity between CAVs. Next, the algorithm initializes the subgraphs and a visited array to keep track of visited CAVs. It iterates through each CAV in \mathcal{V} and checks if it has been visited. If not, a new subgraph \mathcal{H} is created with the current CAV as the starting node. The node is marked as visited and a queue is initialized with the current CAV. Within the “while” loop, the algorithm retrieves a node n^j from the queue along with its neighbors. For each neighbor that has not been visited, it is added to the subgraph \mathcal{H} and the queue. The neighbor is also marked as visited. This process continues until the queue is \emptyset . Finally, the algorithm create the edges of each subgraph and store it to the list of subgraphs $\mathcal{H}^1, \mathcal{H}^2, \dots, \mathcal{H}^K$. This process repeats until all CAVs have been visited, resulting in a collection of subgraphs. Within one set of nodes created by Algorithm 3, the edges to construct the subgraph $\mathcal{H}(\mathcal{N}, \mathcal{E}_h)$ between node pairs are created by:

$$\mathcal{E}_h = \{(n^i, n^j), j \in \mathcal{N} | d^{i,j} \leq r_{\text{tele}}^i\}. \quad (43)$$

Remark 7. Algorithm 3 provides a foundation for the construction of decentralized cooperative motion planning problems by maintaining the adjacency matrix A_G among CAVs. These sets of nodes \mathcal{N}^k serve as the basis for CAV coordination in the subsequent stages of the motion planning process.

B. Large-Scale Cooperative Motion Planning with Receding Horizon and Graph Evolution

The pipeline of the proposed cooperative motion planning framework involves optimizing the trajectories of the CAVs in a planning horizon of T_s and executing only the first T_e

Algorithm 4 Large-Scale Cooperative Motion Planning with Receding Horizon and Graph Evolution

- 1: **obtain** starting and target positions of all CAVs in \mathcal{G}
 - 2: **determine** optimal route using A* algorithm
 - 3: **smooth** the waypoints in each route using the Savitzky-Golay filter
 - 4: **while** termination criterion is not satisfied **do**:
 - 5: Execute Algorithm 3 to distribute the CAVs to \mathcal{H}^k
 - 6: **for** subgraph \mathcal{H} in subgraphs list **do**
 - 7: **formulate** the OCP (28) for the CAVs in \mathcal{H}
 - 8: **search** nearest waypoints for each CAV at each time step $\tau \in \{0, 1, \dots, T_s\}$ using KD-Tree
 - 9: Execute Algorithm 2 to obtain CAVs' trajectories
 - 10: **end for**
 - 11: **perform** first T_e steps of the CAVs in \mathcal{G}
 - 12: **feedback** at time step T_e
 - 13: **relay** the states of all the CAVs in \mathcal{G}
 - 14: **end while**
-

steps. We set $T_s > T_e$, which can cater to uncertainties and dynamics faults during the $(T_s - T_e)$ time horizon constructing a closed-loop structure. Besides, the horizon of the whole driving process from the starting point to the destination is denoted as T . With a receding horizon manner, it is not necessary to detect vehicles that are far away, because the maximum velocity of each CAV is limited, which defines a boundary for the trip distance within the limited planning horizon. This feature benefits the graph evolution algorithm to construct more subgraphs to effectively control the scale of the OCPs corresponding to each subgraph.

The cooperative motion planning strategy with a receding horizon is presented in Algorithm 4. Initially, the starting and target positions of all CAVs are determined by users. A preliminary route with guidance waypoints is generated and smoothed based on the road topology provided by the OpenDRIVE map, using the A* algorithm and the Savitzky-Golay filter. In the “while” loop, the graph evolution is performed using Algorithm 3, and OCPs are formulated within each subgraph. To facilitate cooperative maneuvers, the nearest neighbor search is performed using an efficient KD-Tree structure within the subsequent T_s steps. After formulating the decentralized cooperative motion planning optimization problem and parallelly executing Algorithm 2 for each subgraph \mathcal{H} , the trajectories of all CAVs are obtained. The first T_e trajectories of the CAVs are executed, and the state and environment feedback at time step T_e is collected and relayed between the CAVs. Simultaneously, \mathcal{G} is updated by Algorithm 3. The aforementioned steps are repeated to obtain the remaining trajectories during T_e to T .

VI. SIMULATION RESULTS

A. Environment Setup

We implement the proposed efficient decentralized cooperative motion planning framework in Ubuntu 20.04 LTS with Intel(R) Xeon(R) Gold 6230 CPU @ 2.10GHz CPU and NVIDIA TITAN RTX GPU with 256 GB RAM and

24 × 4 GB Graphic Memory. We perform the algorithms using Python 3.8 with Numba acceleration. The simulation platform is CARLA 0.9.14 [42] with TOWN05. The pertinent parameters of the CAVs are depicted in Table I. It is notable that $d^{i,1} = -0.28$ m means that the rear circle of the target vehicle is in front of the virtual center (center of the rear axle) of the vehicle model (2). In the remainder of this section, we conduct two

TABLE I
PARAMETER SETTINGS OF THE CAVS

Param.	Description	Value	Param.	Description	Value
b	wheelbase	2.4 m	$d^{i,1}$	rear distance	-0.28 m
l	vehicle length	3.8 m	a^j	semi-major	3 m
w	vehicle width	1.7 m	b^j	semi-minor	1.1 m
$d^{i,0}$	front distance	2.68 m	r^i	radius	2.55 m

sets of simulation experiments to evaluate the computational efficiency of the proposed optimization algorithm and the driving performance of the proposed decentralized cooperative motion planning strategy, respectively.

We use the same guidance trajectories of the CAVs in the same map for all the benchmark methods in the comparative experiment. Concretely, as shown in Table II, we adopt different hyper-parameters for the reference trajectories generation of different scales of CAVs. The CAVs' spawn points $z_{\text{ref},0}^i$ and destinations $z_{\text{ref},T}^i$ are randomly generated. Afterward, the rough guidance trajectories containing waypoints $z_{\text{ref},\tau}^i, \tau \in [1, 2, \dots, T]$ are searched as described by Section IV-A. The generated spawn points are within a range of $[d_{\min}, d_{\max}]$ from $(-188 \text{ m}, -91.5 \text{ m})$, the center position of an intersection in TOWN 05, while the destinations of CAVs are within a range of $[d_{\text{des},\min}, d_{\text{des},\max}]$ from their spawn points $z_{\text{ref},0}^i$. Lastly, to simulate real urban driving scenarios, the target velocity of each CAV v_{ref}^i is randomly assigned between $[v_{\min}, v_{\max}]$.

TABLE II
PARAMETERS FOR DRIVING SCENARIO CONSTRUCTION

# CAV	d_{\min}	d_{\max}	$d_{\text{des},\min}$	$d_{\text{des},\max}$	v_{\min}	v_{\max}
8	7.5 m	30.0 m	100.0 m	150.0 m	10.0 m/s	10.0 m/s
16	7.5 m	70.0 m	100.0 m	150.0 m	5.0 m/s	20.0 m/s
32	10.0 m	140.0 m	120.0 m	150.0 m	5.0 m/s	20.0 m/s
80	10.0 m	340.0 m	140.0 m	170.0 m	5.0 m/s	20.0 m/s

B. Cooperative Motion Planning Under One Subgraph

1) *Computational Efficiency Comparison*: We compare our optimization algorithm for solving cooperative motion planning problems with existing commonly used solvers (the IPOPT solver and the SQP solver provided by CasADi [43]) and advanced algorithms (centralized iLQR (CiLQR) with log barrier function [20], and decentralized iLQR (DiLQR) with soft collision avoidance [26]). The hyper-parameters of the optimization algorithms are listed in Table III.

Computation time of different optimization horizons (T) and CAV numbers (N) are compared using a static CAV graph \mathcal{G} without graph evolution. As depicted in Table IV, we compare the computation time of various optimization algorithms with

TABLE III
PARAMETER SETTINGS OF THE OPTIMIZATION ALGORITHMS

Parameter	Value	Parameter	Value	Parameter	Value
σ	0.05	τ_s	0.1 s	φ_b	0.6 rad
ρ	0.002	a_{\max}	3.0 m/s ²	T_s	15
ϵ	0.1	a_{\min}	-5.0 m/s ²	T_e	10

a planning horizon (T_s) ranging from 30 to 90 and a fixed CAV number ($N = 8$). IPOPT and SQP, typical solving methods in CasADi, have high computation time and low efficiency for CAVs' motion planning tasks. SQP struggles with planning horizons greater than 40. CiLQR is more time-efficient due to iterative linearization but faces significantly increased computation time as the planning horizon grows. In contrast, DiLQR, which uses ADMM to decentralize the problem, maintains efficiency even with an increased planning horizon scale. Our proposed method has also high computational efficiency with a larger planning horizon. From another perspective, as shown in Table V, for most of the compared methods, a higher number of CAVs has a greater impact on the computational efficiency than a greater planning horizon. In particular, DiLQR is much less scalable than our improved consensus ADMM algorithm.

TABLE IV
COMPUTATION TIME WITH DIFFERENT OPTIMIZATION HORIZONS

Method	Optimization horizon with $N = 8$						
	30	40	50	60	70	80	90
CiLQR [20]	0.276	0.361	0.577	1.314	2.031	1.413	2.099
IPOPT [43]	4.311	8.701	18.602	31.630	95.909	—	—
SQP [43]	758.680	—	—	—	—	—	—
DiLQR [26]	0.398	0.339	0.614	0.582	0.713	1.069	1.473
Ours	0.197	0.377	0.407	0.550	0.733	1.035	1.434

TABLE V
COMPUTATION TIME WITH DIFFERENT NUMBERS OF CAVS

Method	Number of CAVs with $T = 30$							
	4	8	12	16	20	24	28	32
CiLQR [20]	0.157	0.276	1.763	6.001	16.901	15.888	19.395	20.110
IPOPT [43]	0.935	4.311	130.961	173.720	314.550	—	—	—
SQP [43]	124.320	758.680	—	—	—	—	—	—
DiLQR [26]	0.073	0.398	0.301	0.490	1.096	3.343	5.146	5.419
Ours	0.152	0.197	0.565	0.792	0.364	1.159	1.887	2.522

2) *Driving Performance Analysis*: As the cooperative motion planning problem (4) is non-convex, it is challenging to guarantee finding the global optimal solution using any solver. Therefore, it becomes necessary to establish evaluation criteria to assess the optimization performance. In this paper, the motion planning performance is evaluated based on two criteria: the minimum distance between any pair of CAVs and the velocity distribution throughout the entire driving process.

As depicted in Fig. 4, all the methods exhibit a similar trend and successfully achieve safe driving performance in terms of the minimum distance between CAVs. However, when considering driving efficiency, notable differences arise among the methods. As demonstrated in Fig. 5, the SQP method exhibits the largest deviation and variance from the reference velocity, with the lowest mean velocity among all

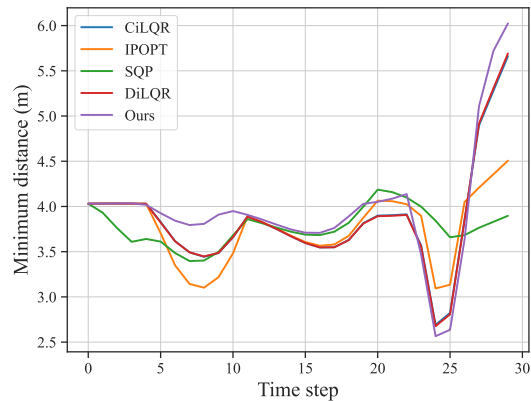


Fig. 4. The minimum distance between all the CAVs at each time step. Different colors represent different methods. All the above methods performed safe cooperative motion planning with a minimum distance greater than 2.5 m.

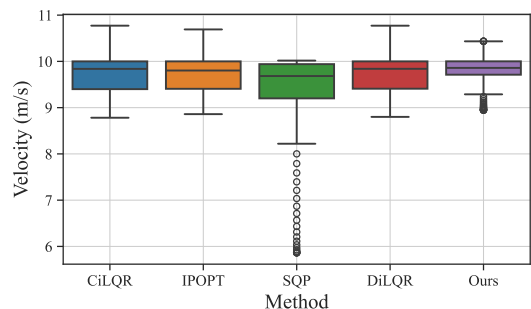


Fig. 5. Velocity distribution along all the time steps with different methods. As the reference velocity is 10 m/s, a speed distribution closer to this value indicates better driving performance.

the alternatives. Compared with other algorithms, our proposed method demonstrates minimal variance, coupled with a relatively high average velocity. In summary, our proposed cooperative optimization algorithm outperforms other methods in terms of scalability, safety, and traveling efficiency. It showcases robustness against an increase in the planning horizon and the number of CAVs.

Note that when the number of CAVs involved in one OCP is more than 20, the cooperative optimization problem consumes more than 1.0 s, which is not sufficient for real-time urban cooperative driving tasks. Hence, our proposed graph evolution algorithm is tailored for the context of large-scale cooperative motion planning, which we thoroughly examine in the subsequent part.

C. Large-Scale Cooperative Motion Planning

In this section, we implement closed-loop cooperative motion planning framework for large-scale CAVs. The objectives of this experiment are to evaluate the robustness, scalability, and effectiveness of the proposed cooperative motion planning framework including the graph evolution and receding horizon strategies. We analyze node distribution situations and qualitative rationality of the CAVs' behavior. To achieve this, we construct a randomly generated large-scale urban driving scenario containing 80 CAVs with varied target velocities

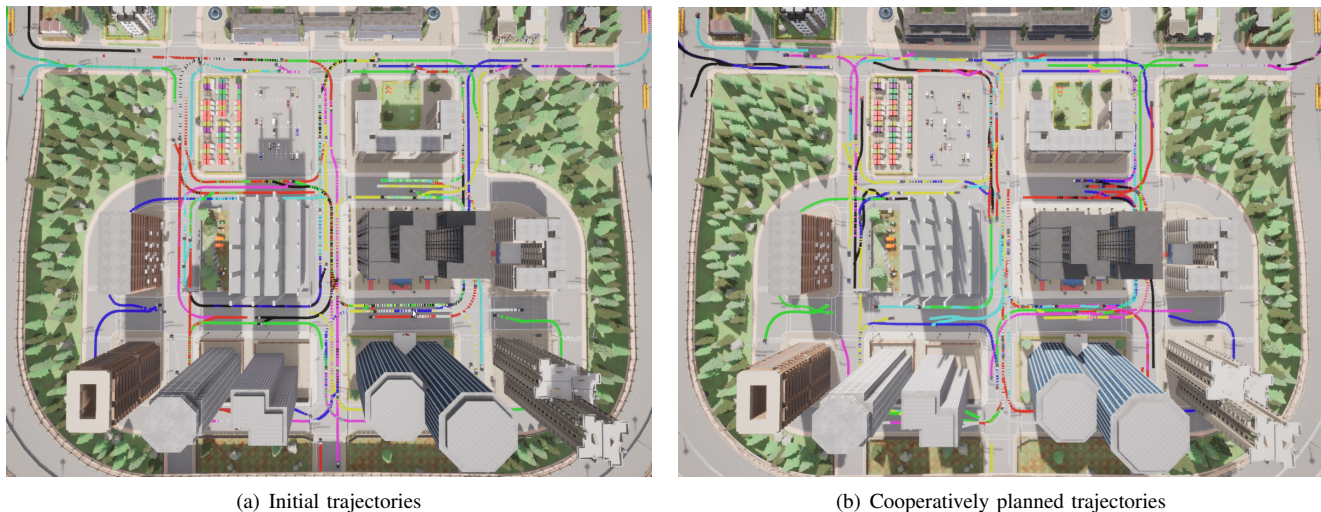


Fig. 6. Rough guidance trajectories and cooperatively planned trajectories for 80 CAVs in the Town 05. Different colors represent the trajectories for different CAVs. Note that there are many potential collision regions in the rough guidance trajectories.

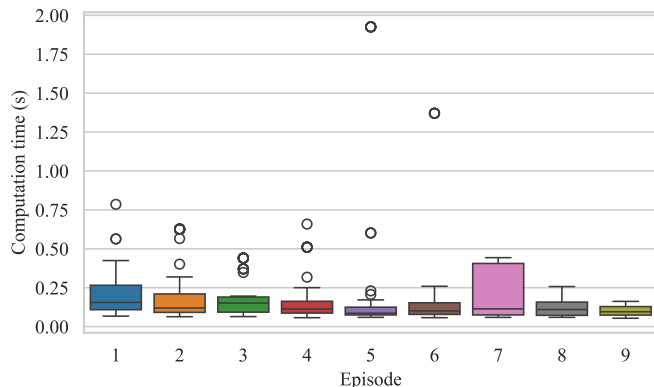


Fig. 7. Computation time for each CAV in all the subgraphs. Most of the problems can be solved within 0.25 seconds, and the computation time has a small standard deviation.

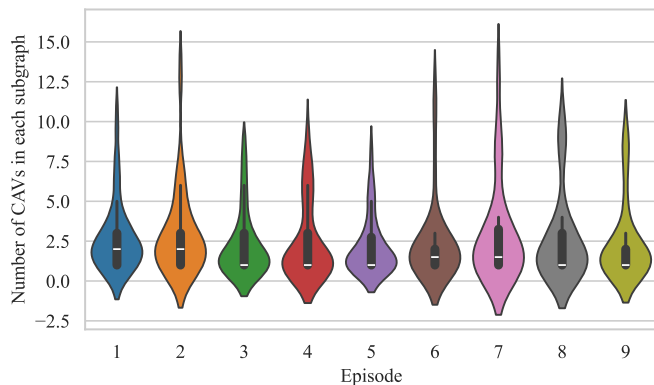


Fig. 8. The number of CAVs in each subgraph within different episodes in the proposed cooperative motion planning framework.

as depicted in Table II. The guidance trajectories of the CAVs in this scenario are shown in Fig. 6(a). This random scenario generation setting enables us to simulate complex urban driving tasks and validate the framework's robustness.

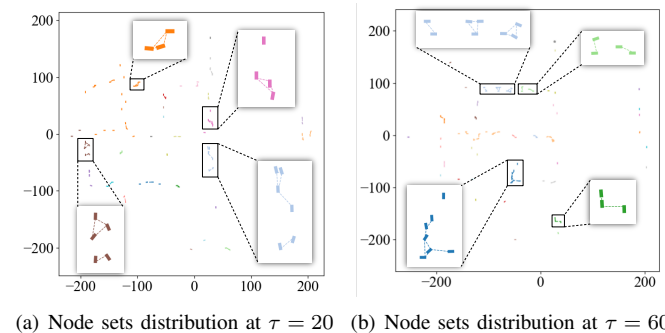


Fig. 9. Node sets distribution at different time steps. Different color means different node sets of CAVs, and the dashed lines between each pair of vehicles mean the communication ability with each other.

We use a receding horizon strategy with a control horizon of $T_e = 10$ and planning horizon of $T_s = 15$.

1) *Effectiveness Analysis of the Node Distribution*: Fig. 7 depicts the computation time in each episode for the planning horizon within each subgraph \mathcal{H} generated from the dynamic connectivity graph \mathcal{G} of the 80 CAVs. In most cases, the computation time is less than 0.25 s with a small standard variance, which indicates that the computation time of the algorithm does not fluctuate much under various urban driving conditions and real-time planning can be achieved.

Note that such stable and efficient computing time is inseparable from our proposed graph evolution algorithm. With this, the subsets of CAVs \mathcal{N} are redistributed and updated with an appropriate size through the whole cooperative driving process. As demonstrated in Fig. 8 and Fig. 9, the sizes of the subgraphs, determined using the proposed conditional Manhattan distance, are relatively small with less than 10 CAVs. Note that in moments with high CAV density, such as at intersections or long queues on a straight road, the scale of the subgraphs increases slightly, such as the subgraph distribution of CAVs at $\tau = 60$ in Fig. 9(b), which is the main reason for the several high computation time recorded in Fig. 7.

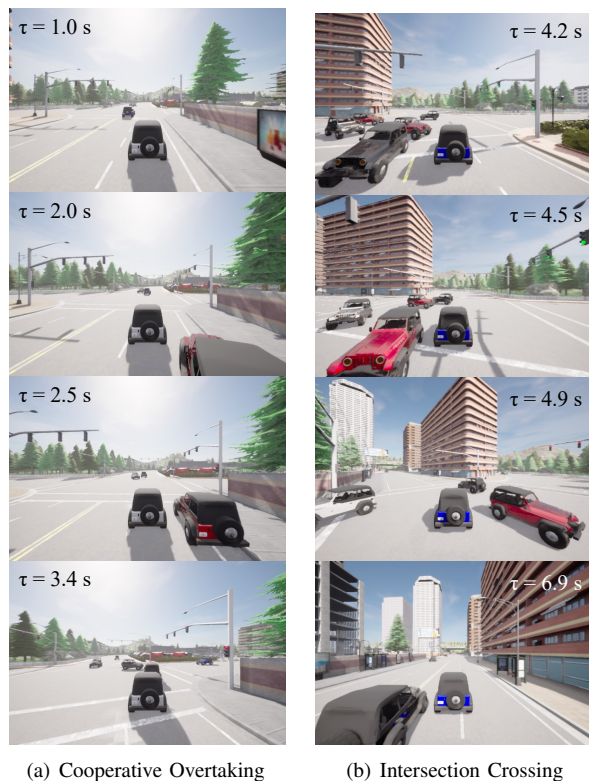


Fig. 10. Driving performance in two challenging scenarios simulated in CARLA. In (a), the red CAV overtakes the leading one with minor steering and deviation from its road lane holding a narrow safety distance, due to the slight avoidance of the leading vehicle. In (b), all the CAVs collaboratively drive with a relatively high safety distance without collision in dense conditions.

2) *Cooperative Driving Performance Evaluation:* In this part, we thoroughly evaluate the cooperative driving performance in the high-fidelity urban traffic scenario, taking into account safety and rationality indices. A comparison between the initial trajectories and the cooperatively optimized driving trajectories shown in Fig. 6 reveals that the optimized trajectories exhibit more curves, even on straight road lanes. This can be attributed to the overtaking and active avoidance behaviors of the CAVs. It is worth noting that these trajectories are sufficiently smooth, allowing the CAVs to adjust their heading angles θ_τ^i with slight steering φ_τ^i , thereby enhancing the comfort of passengers in CAVs within the traffic system.

For typical and challenging situations, such as overtaking or intersection areas, CAVs exhibit a proactive inclination to evade one another, thereby enhancing both driving effectiveness and safety performance. A notable illustration can be observed in Fig. 10(a), where the red CAV successfully executes an overtaking maneuver without compromising driving efficiency, due to the active avoidance of the white CAV on the left. Another noteworthy challenge in urban driving pertains to navigating intersections. As depicted in Fig. 10(b), all the CAVs efficiently drive without stopping and giving way to others in the unsignalized intersection, obviously increasing the traveling efficiency. The reasons for the above safe and efficient driving performance are the adoption of a cooperative motion planning optimization strategy, aligned with the driving strategy outlined in Algorithm 4 and the utilization of an

appropriate CAV scale within each subgraph.

VII. CONCLUSION

In this work, a comprehensive cooperative motion planning framework is devised to address the cooperative motion planning problem in large-scale traffic scenarios involving excessive numbers of CAVs. This framework integrates trajectory generation, graph evolution, and parallel optimization for cooperative urban driving. We enhance computational efficiency of the dual consensus ADMM, by leveraging the sparsity in the dual update of box constraints. The introduction of a graph evolution strategy with the receding horizon effectively manages the scale of each OCP in each subgraph \mathcal{H} , regardless of the number of CAVs in graph \mathcal{G} . The simulation results of cooperative motion planning within one subgraph showcase the superiority of the proposed improved consensus ADMM in terms of computational efficiency and driving efficiency, especially with higher planning horizons and increasing numbers of CAVs. We also conduct comprehensive simulations for cooperative motion planning tasks involving 80 CAVs. With the proposed methodology, the computation time for the problem is maintained to be under 0.5 s in most instances. The CAVs exhibit exceptional cooperation behaviors in different driving scenarios. These findings effectively showcase the capabilities of the proposed cooperative driving framework in managing large-scale CAVs, offering valuable insights for efficient coordination in modern transportation networks.

REFERENCES

- [1] C. Chang, J. Zhang, K. Zhang, W. Zhong, X. Peng, S. Li, and L. Li, "BEV-V2X: Cooperative birds-eye-view fusion and grid occupancy prediction via V2X-based data sharing," *IEEE Transactions on Intelligent Vehicles*, vol. 8, no. 11, pp. 4498–4514, 2023.
- [2] M. Wegener, F. Herrmann, L. Koch, R. Savelsberg, and J. Andert, "Longitudinal vehicle motion prediction in urban settings with traffic light interaction," *IEEE Transactions on Intelligent Vehicles*, vol. 8, no. 1, pp. 204–215, 2023.
- [3] C. Toumeh and A. Lambert, "Decentralized multi-agent planning using model predictive control and time-aware safe corridors," *IEEE Robotics and Automation Letters*, vol. 7, no. 4, pp. 1110–1117, 2022.
- [4] W. Xiao, H. Ren, Q. Zhou, H. Li, and R. Lu, "Distributed finite-time containment control for nonlinear multiagent systems with mismatched disturbances," *IEEE Transactions on Cybernetics*, vol. 52, no. 7, pp. 6939–6948, 2022.
- [5] L.-H. Wen and K.-H. Jo, "Deep learning-based perception systems for autonomous driving: A comprehensive survey," *Neurocomputing*, vol. 489, pp. 255–270, 2022.
- [6] L. Zhang, Z. Hou, J. Wang, Z. Liu, and W. Li, "Robot navigation with reinforcement learned path generation and fine-tuned motion control," *IEEE Robotics and Automation Letters*, vol. 8, no. 8, pp. 4489–4496, 2023.
- [7] X. Duan, C. Sun, D. Tian, J. Zhou, and D. Cao, "Cooperative lane-change motion planning for connected and automated vehicle platoons in multi-lane scenarios," *IEEE Transactions on Intelligent Transportation Systems*, vol. 24, no. 7, pp. 7073–7091, 2023.
- [8] C. Hu, Z. Wang, H. Taghavifar, J. Na, Y. Qin, J. Guo, and C. Wei, "MME-EKF-Based path-tracking control of autonomous vehicles considering input saturation," *IEEE Transactions on Vehicular Technology*, vol. 68, no. 6, pp. 5246–5259, 2019.
- [9] L. Claussmann, M. Revilloud, D. Gruyer, and S. Glaser, "A review of motion planning for highway autonomous driving," *IEEE Transactions on Intelligent Transportation Systems*, vol. 21, no. 5, pp. 1826–1848, 2020.
- [10] S. Teng, X. Hu, P. Deng, B. Li, Y. Li, Y. Ai, D. Yang, L. Li, Z. Xuanyuan, F. Zhu, *et al.*, "Motion planning for autonomous driving: The state of the art and future perspectives," *IEEE Transactions on Intelligent Vehicles*, 2023.

- [11] J. Duan, J. Li, Q. Ge, S. E. Li, M. Bujarbaruah, F. Ma, and D. Zhang, "Relaxed actor-critic with convergence guarantees for continuous-time optimal control of nonlinear systems," *IEEE Transactions on Intelligent Vehicles*, vol. 8, no. 5, pp. 3299–3311, 2023.
- [12] G. Sartoretti, J. Kerr, Y. Shi, G. Wagner, T. S. Kumar, S. Koenig, and H. Choset, "PRIMAL: Pathfinding via reinforcement and imitation multi-agent learning," *IEEE Robotics and Automation Letters*, vol. 4, no. 3, pp. 2378–2385, 2019.
- [13] H. Liu, Z. Qu, and R. Zhu, "Solving a multi-robot search problem with bionic SARSA algorithm and artificial potential field," in *2021 China Automation Congress (CAC)*, pp. 1830–1835, IEEE, 2021.
- [14] M. Klimke, B. Völz, and M. Buchholz, "Cooperative behavior planning for automated driving using graph neural networks," in *2022 IEEE Intelligent Vehicles Symposium (IV)*, pp. 167–174, IEEE, 2022.
- [15] B. Wang, X. Gong, Y. Wang, P. Lyu, and S. Liang, "Coordination for connected and autonomous vehicles at unsignalized intersections: An iterative learning based collision-free motion planning method," *IEEE Internet of Things Journal*, 2023.
- [16] B. Li, T. Acarman, Y. Zhang, Y. Ouyang, C. Yaman, Q. Kong, X. Zhong, and X. Peng, "Optimization-based trajectory planning for autonomous parking with irregularly placed obstacles: A lightweight iterative framework," *IEEE Transactions on Intelligent Transportation Systems*, vol. 23, no. 8, pp. 11970–11981, 2022.
- [17] Y. Lee, M. Cho, and K.-S. Kim, "GPU-parallelized iterative LQR with input constraints for fast collision avoidance of autonomous vehicles," in *2022 IEEE/RSJ International Conference on Intelligent Robots and Systems (IROS)*, pp. 4797–4804, IEEE, 2022.
- [18] C. Mastalli, W. Merkt, J. Marti-Saumell, H. Ferrolho, J. Solà, N. Mansard, and S. Vijayakumar, "A feasibility-driven approach to control-limited DDP," *Autonomous Robots*, vol. 46, no. 8, pp. 985–1005, 2022.
- [19] Y. Aoyama, G. Boutselis, A. Patel, and E. A. Theodorou, "Constrained differential dynamic programming revisited," in *2021 IEEE International Conference on Robotics and Automation (ICRA)*, pp. 9738–9744, IEEE, 2021.
- [20] J. Chen, W. Zhan, and M. Tomizuka, "Autonomous driving motion planning with constrained iterative LQR," *IEEE Transactions on Intelligent Vehicles*, vol. 4, no. 2, pp. 244–254, 2019.
- [21] J. Ma, Z. Cheng, X. Zhang, M. Tomizuka, and T. H. Lee, "Alternating direction method of multipliers for constrained iterative LQR in autonomous driving," *IEEE Transactions on Intelligent Transportation Systems*, vol. 23, no. 12, pp. 23031–23042, 2022.
- [22] J. Ma, Z. Cheng, X. Zhang, Z. Lin, F. L. Lewis, and T. H. Lee, "Local learning enabled iterative linear quadratic regulator for constrained trajectory planning," *IEEE Transactions on Neural Networks and Learning Systems*, vol. 34, no. 9, pp. 5354–5365, 2023.
- [23] S. Boyd, N. Parikh, E. Chu, B. Peleato, J. Eckstein, *et al.*, "Distributed optimization and statistical learning via the alternating direction method of multipliers," *Foundations and Trends in Machine Learning*, vol. 3, no. 1, pp. 1–122, 2011.
- [24] X. Zhang, Z. Cheng, J. Ma, S. Huang, F. L. Lewis, and T. H. Lee, "Semi-definite relaxation-based ADMM for cooperative planning and control of connected autonomous vehicles," *IEEE Transactions on Intelligent Transportation Systems*, vol. 23, no. 7, pp. 9240–9251, 2021.
- [25] G. Banjac, F. Rey, P. Goulart, and J. Lygeros, "Decentralized resource allocation via dual consensus ADMM," in *2019 American Control Conference (ACC)*, pp. 2789–2794, IEEE, 2019.
- [26] Z. Huang, S. Shen, and J. Ma, "Decentralized iLQR for cooperative trajectory planning of connected autonomous vehicles via dual consensus ADMM," *IEEE Transactions on Intelligent Transportation Systems*, 2023.
- [27] J. Ye, L. Xiang, and X. Ge, "Spatial-temporal modeling and analysis of reliability and delay in urban V2X networks," *IEEE Transactions on Network Science and Engineering*, 2023.
- [28] A. I. Rikos, W. Jiang, T. Charalambous, and K. H. Johansson, "Asynchronous distributed optimization via ADMM with efficient communication," *arXiv preprint arXiv:2309.04585*, 2023.
- [29] O. Shorinwa, T. Halsted, and M. Schwager, "Scalable distributed optimization with separable variables in multi-agent networks," in *2020 American Control Conference (ACC)*, pp. 3619–3626, IEEE, 2020.
- [30] A. D. Saravanos, Y. Aoyama, H. Zhu, and E. A. Theodorou, "Distributed differential dynamic programming architectures for large-scale multi-agent control," *IEEE Transactions on Robotics*, 2023.
- [31] Z. Sheng, Y. Xu, S. Xue, and D. Li, "Graph-based spatial-temporal convolutional network for vehicle trajectory prediction in autonomous driving," *IEEE Transactions on Intelligent Transportation Systems*, vol. 23, no. 10, pp. 17654–17665, 2022.
- [32] T. Brüdigan, M. Olbrich, D. Wollherr, and M. Leibold, "Stochastic model predictive control with a safety guarantee for automated driving," *IEEE Transactions on Intelligent Vehicles*, 2021.
- [33] H. Liu, K. Chen, Y. Li, Z. Huang, J. Duan, and J. Ma, "Integrated behavior planning and motion control for autonomous vehicles with traffic rules compliance," in *2023 IEEE International Conference on Robotics and Biomimetics (ROBIO)*, pp. 1995–2002, IEEE, 2023.
- [34] Y. Qu, H. Chu, S. Gao, J. Guan, H. Yan, L. Xiao, S. E. Li, and J. Duan, "RL-driven MPPI: Accelerating online control laws calculation with offline policy," *IEEE Transactions on Intelligent Vehicles*, pp. 1–12, 2023.
- [35] C. E. Luis, M. Vukosavljev, and A. P. Schoellig, "Online trajectory generation with distributed model predictive control for multi-robot motion planning," *IEEE Robotics and Automation Letters*, vol. 5, no. 2, pp. 604–611, 2020.
- [36] D. Qin, Z. Jin, A. Liu, W.-A. Zhang, and L. Yu, "Asynchronous event-triggered distributed predictive control for multi-agent systems with parameterized synchronization constraints," *IEEE Transactions on Automatic Control*, 2023.
- [37] Z. Cheng, J. Ma, X. Zhang, C. W. de Silva, and T. H. Lee, "ADMM-based parallel optimization for multi-agent collision-free model predictive control," *arXiv preprint arXiv:2101.09894*, 2021.
- [38] Y. Tassa, N. Mansard, and E. Todorov, "Control-limited differential dynamic programming," in *2014 IEEE International Conference on Robotics and Automation (ICRA)*, pp. 1168–1175, IEEE, 2014.
- [39] W. Schwarting, J. Alonso-Mora, L. Paull, S. Karaman, and D. Rus, "Safe nonlinear trajectory generation for parallel autonomy with a dynamic vehicle model," *IEEE Transactions on Intelligent Transportation Systems*, vol. 19, no. 9, pp. 2994–3008, 2017.
- [40] P. D. Grontas, M. W. Fisher, and F. Dörfler, "Distributed and constrained H_2 control design via system level synthesis and dual consensus ADMM," in *2022 IEEE 61st Conference on Decision and Control (CDC)*, pp. 301–307, IEEE, 2022.
- [41] H. Bauschke and P. Combettes, "Convex analysis and monotone operator theory in Hilbert spaces," *CMS books in mathematics*, vol. 10, pp. 978–1, 2011.
- [42] A. Dosovitskiy, G. Ros, F. Codevilla, A. Lopez, and V. Koltun, "CARLA: An open urban driving simulator," in *Conference on Robot Learning*, pp. 1–16, PMLR, 2017.
- [43] J. A. Andersson, J. Gillis, G. Horn, J. B. Rawlings, and M. Diehl, "CasADi: a software framework for nonlinear optimization and optimal control," *Mathematical Programming Computation*, vol. 11, no. 1, pp. 1–36, 2019.